Article

Rifaximin prophylaxis causes resistance to the last-resort antibiotic daptomycin

https://doi.org/10.1038/s41586-024-08095-4

Received: 25 July 2022

Accepted: 20 September 2024

Published online: 23 October 2024

Open access

Check for updates

Adrianna M. Turner[1], Lucy Li[1], Ian R. Monk[1], Jean Y. H. Lee[1,2], Danielle J. Ingle[1], Stephanie Portelli[3,4], Norelle L. Sherry[1,5,6], Nicole Isles[1], Torsten Seemann[1,5,7], Liam K. Sharkey[1], Calum J. Walsh[1,7], Gavin E. Reid[8,9,10], Shuai Nie[11], Bart A. Eijkelkamp[12], Natasha E. Holmes[6,13], Brennan Collis[6], Sara Vogrin[6,14], Andreas Hiergeist[15], Daniela Weber[16], Andre Gessner[15], Ernst Holler[16], David B. Ascher[3,4], Sebastian Duchene[1,17], Nichollas E. Scott[1], Timothy P. Stinear[1,7], Jason C. Kwong[1,6], Claire L. Gorrie[1,5,7,18], Benjamin P. Howden[1,5,6,7,18] ✉ & Glen P. Carter[1,7,18] ✉

Multidrug-resistant bacterial pathogens like vancomycin-resistant *Enterococcus faecium* (VREfm) are a critical threat to human health[1]. Daptomycin is a last-resort antibiotic for VREfm infections with a novel mode of action[2], but for which resistance has been widely reported but is unexplained. Here we show that rifaximin, an unrelated antibiotic used prophylactically to prevent hepatic encephalopathy in patients with liver disease[3], causes cross-resistance to daptomycin in VREfm. Amino acid changes arising within the bacterial RNA polymerase in response to rifaximin exposure cause upregulation of a previously uncharacterized operon (*prdRAB*) that leads to cell membrane remodelling and cross-resistance to daptomycin through reduced binding of the antibiotic. VREfm with these mutations are spread globally, making this a major mechanism of resistance. Rifaximin has been considered 'low risk' for the development of antibiotic resistance. Our study shows that this assumption is flawed and that widespread rifaximin use, particularly in patients with liver cirrhosis, may be compromising the clinical use of daptomycin, a major last-resort intervention for multidrug-resistant pathogens. These findings demonstrate how unanticipated antibiotic cross-resistance can undermine global strategies designed to preserve the clinical use of critical antibiotics.

Antimicrobial resistance (AMR) is one of the greatest current public health threats, with 1.27 million deaths being attributed to bacterial AMR in 2019[1]. Infections caused by multidrug-resistant bacteria are associated with frequent treatment failure and high rates of morbidity and mortality; the preservation of last-resort antibiotics for effective treatment is therefore of critical importance.

E. faecium is classified by the World Health Organization (WHO) as a high-priority pathogen as it is a leading cause of nosocomial infections[4]. The intrinsic antibiotic resistance of hospital-associated clones coupled with their ability to rapidly acquire additional antibiotic-resistance genes makes *E. faecium* infections increasingly difficult to treat[5]. In particular, strains resistant to vancomycin, the first-line antibiotic for invasive infections, have emerged and disseminated globally due to the acquisition of transferable *van* resistance genes[6].

The lipopeptide daptomycin (DAP) is a WHO-designated last-resort antibiotic that is used 'off label' to treat invasive VREfm infections[7]. The increasing reports of DAP-resistant (DAP-R) VREfm are therefore of clinical concern. In VREfm, DAP resistance is thought to be largely driven by mutations in the regulatory systems LiaFSR/LiaXYZ and in the cardiolipin synthase (Cls)[8–10]. However, many VREfm are resistant to DAP through unknown mechanisms, indicating that other molecular pathways are involved[9,11,12]. Accordingly, we undertook a combined genomic and phenotypic analysis to investigate the DAP resistance mechanisms in VREfm. Here we show that DAP resistance is linked to the presence of specific *rpoB* mutations in VREfm, with resistance emerging de novo in *E. faecium* after exposure to rifaximin, a commonly prescribed antibiotic that is used prophylactically to prevent hepatic encephalopathy in patients with liver disease[3]. We identify

[1]Department of Microbiology and Immunology, The University of Melbourne at The Peter Doherty Institute for Infection and Immunity, Melbourne, Victoria, Australia. [2]Department of Infectious Diseases, Monash Health, Clayton, Victoria, Australia. [3]Computational Biology and Clinical Informatics, Baker Heart and Diabetes Institute, Melbourne, Victoria, Australia. [4]School of Chemistry and Molecular Biosciences, The University of Queensland, Saint Lucia Campus, Saint Lucia, Queensland, Australia. [5]Microbiological Diagnostic Unit Public Health Laboratory, Department of Microbiology and Immunology, The University of Melbourne at The Peter Doherty Institute for Infection and Immunity, Melbourne, Victoria, Australia. [6]Department of Infectious Diseases & Immunology, Austin Health, Melbourne, Victoria, Australia. [7]Centre for Pathogen Genomics, The University of Melbourne, Melbourne, Victoria, Australia. [8]School of Chemistry, The University of Melbourne, Melbourne, Victoria, Australia. [9]Department of Biochemistry and Pharmacology, The University of Melbourne, Melbourne, Victoria, Australia. [10]Bio21 Molecular Science and Biotechnology Institute, The University of Melbourne, Melbourne, Victoria, Australia. [11]Melbourne Mass Spectrometry and Proteomics Facility, Bio21 Molecular Science and Biotechnology Institute, The University of Melbourne, Melbourne, Victoria, Australia. [12]Molecular Sciences and Technology, College of Science and Engineering, Flinders University, Adelaide, South Australia, Australia. [13]Department of Infectious Diseases, The University of Melbourne at The Peter Doherty Institute for Infection and Immunity, Melbourne, Victoria, Australia. [14]Department of Medicine, The University of Melbourne, Melbourne, Victoria, Australia. [15]Institute of Clinical Microbiology and Hygiene, University Medical Center, Regensburg, Germany. [16]Department of Internal Medicine III, Hematology and Medical Oncology, University Medical Center, Regensburg, Germany. [17]DEMI Unit, Department of Computational Biology, Institut Pasteur, Paris, France. [18]These authors jointly supervised this work: C. L. Gorrie, B. P. Howden and G. P. Carter. ✉e-mail: bhowden@unimelb.edu.au; glen.carter@unimelb.edu.au

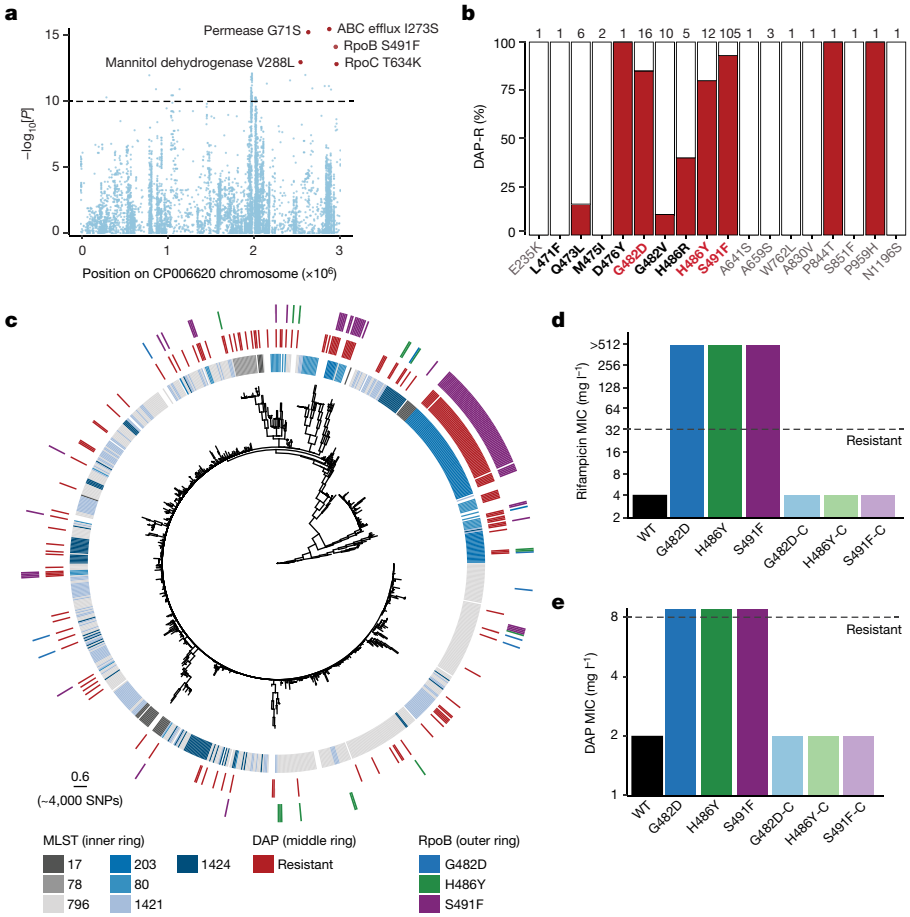

Fig. 1 | Identification of DAP-R RpoB substitutions. a, Manhattan plot of 10,530 variants, displayed by their position on the reference genome and their association with DAP resistance, as determined using one-sided Fisher's exact tests and a mixed-effects logistic regression model to correct for population structure; correction for multiple testing was performed using the Bonferroni method (dashed line). $n = 998$ study isolates and 2 control strains. **b**, The percentage of DAP-R strains with a RpoB substitution; the RRDR is shown in bold. The total number of VREfm containing each mutation is shown. **c**, Maximum-likelihood core-SNP-based phylogeny of clinical VREfm ($n = 998$ study isolates and 2 control strains) inferred from 6,574 SNPs. Overlaid are the results of in silico multi-locus sequence type (MLST), DAP phenotypic testing and RpoB substitutions associated with DAP resistance. In the first circle, ST is not shown for uncommon STs ($n \leq 5$). The scale bar indicates number of nucleotide substitutions per site (top), with an approximation of SNP distance shown in parentheses. **d**, Rifampicin susceptibility testing results for the WT and isogenic *rpoB* mutants and complemented strains (designated by -C). $n = 3$. **e**, DAP susceptibility testing results for the WT and isogenic *rpoB* mutants and complemented strains. $n = 3$. The MIC for each strain is shown without error bars as there was no variation between the independent biological replicates.

a major mechanism of DAP resistance in VREfm and identified rifaximin, an antibiotic considered to be low-risk for the emergence of bacterial AMR[13], as an important driver of last-resort antibiotic resistance.

Australian DAP-R VREfm are polyphyletic

Daptomycin susceptibility testing was performed on VREfm isolated during two unbiased state-wide 'snapshot' studies undertaken in 2015 ($n = 294$) and 2018 ($n = 423$) in Victoria, Australia. The proportion of DAP-R isolates was 16.6% ($n = 49$) in 2015 and 15.3% ($n = 65$) in 2018. Given this high rate of resistance, we included VREfm isolated in 2017 ($n = 108$) and 2018 ($n = 173$)[14,15], and found that 28.4% ($n = 80$) of these isolates were also DAP-R. Overall, a surprisingly high 194 (19.4%) of all VREfm were DAP-R.

To investigate the relationship between DAP-R and DAP-susceptible (DAP-S) VREfm, a maximum-likelihood phylogeny was inferred from an alignment of 6,574 core genome single-nucleotide polymorphisms (SNPs) ($n = 1{,}000$; 998 study isolates and 2 controls) (Extended Data Fig. 1a). We identified 36 sequence types (STs) within the 1,000 isolates and 30 of these STs included at least one DAP-R VREfm; thus, DAP-R was polyphyletic. The largest clade of DAP-R strains (ST203), accounted for 41.2% of resistant isolates ($n = 80$ out of 194) suggestive of an expanding DAP-R lineage. The other predominant VREfm STs (ST80, ST796, ST1421 and ST1424) consisted of several groups of DAP-R isolates that showed no phylogenetic clustering, suggesting that the phenotype has arisen independently on multiple occasions.

We next sought to determine the genetic determinants leading to DAP resistance in VREfm. We systematically screened VREfm genomes for mutations in the regulatory genes *liaFSR*, *liaXYZ*, *yycFG* (*walKR*), cardiolipin synthase *(cls)* and the division site tropomyosin-like locus (*divIVA*), all previously linked to DAP resistance[7,8,16]. Notably, there were no significant associations between DAP resistance and mutations in these loci (Supplementary Table 1).

rpoB mutations lead to DAP resistance in VREfm

To identify genetic loci linked with DAP resistance, we performed a genome-wide association study (GWAS) with the 998 *E. faecium* study isolates and 2 controls (Fig. 1a). This analysis identified 142 mutations (in 73 genes) significantly ($P < 1 \times 10^{-10}$) associated with DAP resistance (as a binary variable with a breakpoint of 8 mg l^{-1}). The top five significant amino acid substitutions were (1) I274S in an uncharacterized ABC

efflux protein ($P = 7.44 \times 10^{-15}$); (2) G71S in an uncharacterized permease protein ($P = 7.77 \times 10^{-14}$); (3) V288L in a mannitol dehydrogenase protein ($P = 6.08 \times 10^{-12}$); (4) S491F in RpoB, the RNA polymerase β subunit ($P = 1.57 \times 10^{-13}$); and (5) T634K in RpoC, the RNA polymerase β′ subunit ($P = 4.40 \times 10^{-11}$).

To test the contribution of these amino acid substitutions to DAP resistance, we introduced each mutation into a clinical DAP-S ST796 VREfm isolate (Aus0233). None of the amino acid substitutions had any impact on DAP resistance except for the S491F substitution within RpoB, which resulted in a DAP-R phenotype (fourfold increase in DAP minimum inhibitory concentration (MIC), from 2 mg l^{-1} to 8 mg l^{-1}). Notably, every clinical strain with the RpoB S491F substitution ($n = 105$, spanning different *E. faecium* genotypes) also contained the RpoC T634K substitution ($n = 105$), with no strains containing the RpoC T634K substitution in isolation. As the T634K substitution did not affect DAP susceptibility (MIC still 8 mg l^{-1}), it might instead be compensatory for negative fitness effects associated with the RpoB S491F substitution. In support of this idea, in vitro competition assays (wild type (WT) versus RpoB(S491F) or WT versus RpoB(S491F)/RpoC(T634K)), showed that the RpoB S491F substitution posed a substantial fitness cost, with a significant ($P < 0.0001$) shift to the WT population (Extended Data Fig. 1b). However, in the RpoB(S491F)/RpoC(T634K) double mutant, the population dynamics remained stable, with no significant differences compared to the inoculum (Extended Data Fig. 1b). These data suggest the RpoC T634K substitution compensates for a negative fitness impact of RpoB S491F.

We next assessed whether other RpoB substitutions were associated with DAP resistance (Fig. 1b). We observed DAP resistance in 81.3% of VREfm strains ($n = 13$ out of 16) with a G482D substitution and 83.3% of VREfm strains ($n = 10$ out of 12) with a H486Y substitution. Isolates containing these mutations were spread across the phylogenetic tree, indicative of multiple independent acquisitions (Fig. 1c). No putative compensatory mutations in the RNA polymerase genes were identified. Clonal expansion was also observed for a dominant, DAP-R clone (ST203) containing the S491F substitution. Daptomycin-resistant isolates from this ST203 lineage were identified across ten geographically distinct hospital networks, indicating that they were not part of a singular hospital outbreak (Extended Data Fig. 1c).

The G482D, H486Y and S491F substitutions were located within the predicted rifampicin-resistance determining region (RRDR) of RpoB (spanning amino acids 467 to 493). Rifampicin susceptibility testing (rifampicin being a marker of rifamycin resistance[17]) confirmed that all of the isolates with a RRDR *rpoB* mutation had high-level rifampicin resistance ($n = 169$; median MIC, 256 mg l^{-1}), while control isolates containing the WT RRDR displayed a median MIC of 8 mg l^{-1} ($n = 169$; Extended Data Fig. 1d).

To test whether the G482D and H486Y substitutions in RpoB also led to rifamycin and DAP resistance we introduced these substitutions into our rifamycin-susceptible, DAP-S, clinical strain of ST796 VREfm (Aus0233). Introduction of the G482D, H486Y or S491F RpoB substitutions resulted in high-level rifampicin resistance (>512 mg l^{-1}) (Fig. 1d). The introduction of the G482D or H486Y RpoB substitutions also resulted in a DAP-R phenotype (fourfold increase in DAP MIC, from 2 mg l^{-1} to 8 mg l^{-1}) (Fig. 1e). Reversing the mutations to recreate the WT *rpoB* allele resulted in susceptibility to rifampicin (MIC of 4 mg l^{-1}) and DAP (MIC of 2 mg l^{-1}), confirming that G482D, H486Y and S491F caused rifamycin resistance and DAP cross-resistance.

VREfm *rpoB* mutations are globally spread

To determine whether the RpoB substitutions associated with DAP resistance observed in Australian VREfm were representative of *E. faecium* globally, we analysed publicly available VREfm genome sequencing data ($n = 3,476$ international and $n = 1,000$ Australian) (Extended Data Fig. 2a). The majority ($n = 3,378$) of these VREfm isolates were healthcare associated, with 98 isolates from animal origin. In total, 630 (14.1%) VREfm isolates had an amino acid substitution in the RRDR of RpoB, with the S491F substitution being the most common, present in 77.9% ($n = 461$) of genomes with a RRDR RpoB substitution (Extended Data Fig. 2b). The S491F substitution was identified in VREfm genomes from 20 countries and across 21 different STs (Extended Data Fig. 2b,c). The G482D and H486Y substitutions were also common, found in 6.8% ($n = 43$) and 11.6% ($n = 73$) of strains with a RpoB substitution, respectively. The G482D and H486Y substitutions were also observed globally (7 and 10 countries, respectively) and across different STs (9 and 22, respectively) (Extended Data Fig. 2b,c). There was a significant association between RRDR RpoB substitutions and healthcare-associated VREfm[18] ($P < 0.001$, Fisher's exact test) (Extended Data Fig. 2d), suggesting that these RpoB substitutions conferring resistance to rifamycins and cross-resistance to DAP are enriched within the healthcare setting and are globally prevalent.

Rifaximin approval linked to S491F emergence

We used phylodynamic analyses to estimate the emergence date of VREfm with the S491F substitution globally. Within Australian VREfm, we observed the expansion of a dominant ST203 clone from 2015 to 2018 that carried the S491F substitution (Fig. 1c). As this clone comprised only *vanA*-VREfm, we genome sequenced all historical *vanA*-VREfm from our public health laboratory ($n = 229$), which consisted of every *vanA*-VREfm isolate collected from 2003 to 2014, to increase the potential to detect a molecular clock signal. We contextualized all Australian isolates ($n = 1,229$) with the international data ($n = 3,476$) and identified three distinct clusters containing the RpoB S491F substitution (Fig. 2a). The same ST203 clone formed the largest cluster (cluster 1; $n = 219$ taxa), consisting of isolates from Australia and the UK. Cluster 2 ($n = 85$ taxa) consisted of ST80 and ST78 isolates from Australia, Europe, South America, the UK and the USA, while cluster 3 ($n = 68$ taxa) consisted of ST80 isolates from Australia, Europe and the UK.

To model the evolutionary trajectories of these clusters, we used core-genome SNP diversity and year of isolation (Extended Data Fig. 3a). The substitution rate (the number of expected nucleotide substitutions per site per year) was consistent with other estimates for healthcare-associated VREfm[18–21] (Fig. 2b). The year of emergence for the most recent common ancestor (MRCA) of each cluster with S491F was around 2006 (Fig. 2b), a time period that coincides with the first clinical use of rifaximin. As rifampicin was approved for clinical use in the USA in 1971[22], several decades before the estimated emergence of the S491F-containing VREfm strains, we considered this rifamycin unlikely to have had a major role in the spread of resistance. Analysis of the three maximum-clade credibility (MCC) trees (Fig. 2b) indicated that each *E. faecium* lineage has continued to expand since its emergence, consistent with the growing use of rifaximin globally, in particular since 2010 when it was approved for the prevention of hepatic encephalopathy[3] (Fig. 2b,c). Notably, in all three VREfm clusters, the S491F substitution has been stably maintained after its acquisition, suggesting sustained selective pressure on the bacterial population, as *rpoB* mutations usually carry a fitness cost[23] (Extended Data Fig. 3b–d). These data show the S491F substitution emerged in VREfm at least three times since the early 2000s, with the predicted dates of emergence closely correlated with the clinical introduction of rifaximin.

Rifaximin linked with DAP-R VREfm carriage

Rifaximin is a non-absorbable oral agent with direct antimicrobial activity in the gastrointestinal tract, predominantly prescribed to prevent recurrent hepatic encephalopathy in patients with liver cirrhosis—a cohort with frequent VREfm gastrointestinal colonization[3,24,25]. As the Bayesian phylodynamic analyses showed a correlation between the

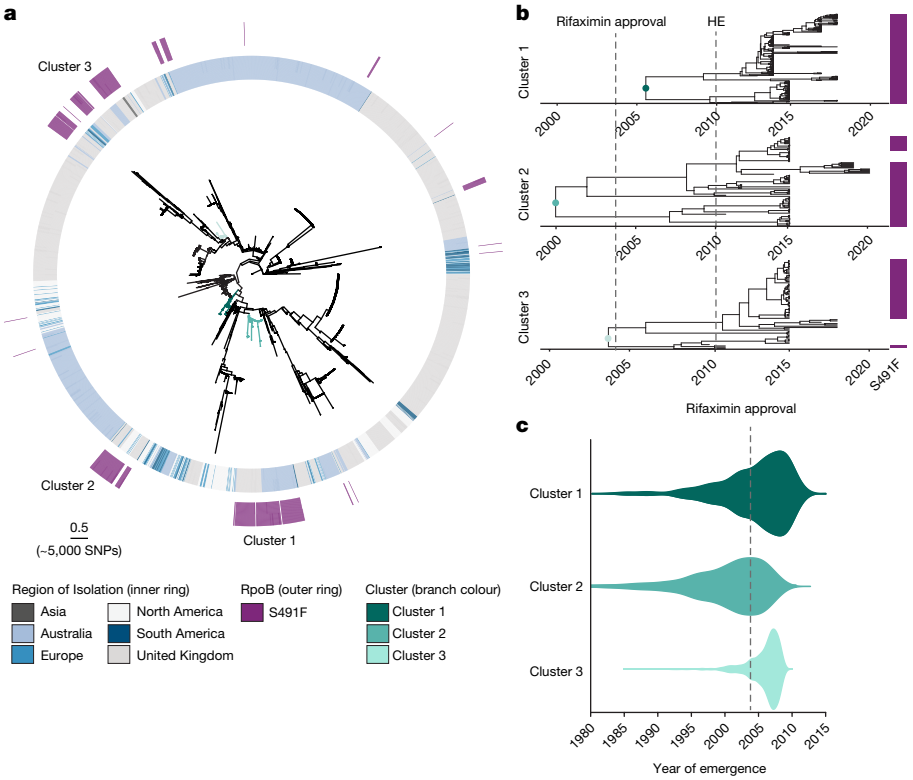

Fig. 2 | Rifaximin approval is linked with the emergence of S491F. **a**, Maximum-likelihood, core-SNP-based phylogeny for 4,476 VREfm inferred from 9,277 core-genome SNPs, demonstrating the presence of the S491F RpoB substitution in international VREfm. Overlaid is the region of isolation for each strain and the presence of the S491F substitution. The coloured branches indicate the three VREfm clusters identified with core genome MLST (cgMLST) used as the input for Bayesian evolutionary analyses. The scale bar indicates the number of nucleotide substitutions per site (top); an approximation of SNP distance is shown in parentheses. **b**, Bayesian phylodynamic analyses showing the MCC trees of the three VREfm clusters with the timing (years on *x* axis) of emergence for each lineage. The presence of the S491F RpoB trait for each isolate is shown in purple. Overlaid onto the MCC trees is the first instance of FDA approval for rifaximin (2004) and for hepatic encephalopathy (HE) (2010). **c**, Violin plots of the most recent common ancestor (MCRA) for each cluster, representing when the RpoB S491F substitution first emerged, with 95% highest-posterior density (HPD) intervals—2006 (HPD 1993–2012) for cluster 1, 2000 (HPD 1989–2008) for cluster 2, and 2004 (HPD 2001–2010) for cluster 3. Overlaid onto violin plots is the FDA approval date for rifaximin (2004).

S491F RpoB substitution in VREfm and the use of rifaximin, we posited that rifaximin use in patients with VREfm colonization may enrich for VREfm RpoB substitutions and, therefore, DAP resistance. To test this hypothesis, we assessed the association between rifaximin exposure and DAP-R VREfm in a retrospective patient cohort at a quaternary referral healthcare centre in Melbourne, Australia (Supplementary Table 2). The *E. faecium* isolates from patients with current or previous rifaximin exposure (rifaximin group) and without previous exposure (control group) were assessed (1) genomically for RpoB substitutions (G482D, H486Y and S491F) that result in DAP resistance; and (2) phenotypically for DAP resistance, by study investigators blinded to patient details and the exposure groups. Genomically clustered isolates likely to represent patient-to-patient transmission were excluded from the analysis, with the included isolates being phylogenetically distributed and representative of *E. faecium* strains identified in state-wide surveys[26] (Methods and Extended Data Fig. 4a).

Among the patient cohort colonized with VREfm, compared with unexposed patients ($n = 116$), patients with recent exposure to rifaximin ($n = 96$) were more likely to be colonized with VREfm with RpoB substitutions ($P < 0.001$), including substitutions associated with DAP resistance (G482D, H486Y or S491F; $P < 0.001$) and DAP-R VREfm ($P < 0.001$) (Fig. 3 and Supplementary Table 3). After adjusting for potential confounding effects, including age, sex, underlying comorbidities and exposure to other antimicrobials, recent rifaximin exposure remained an independent predictor of DAP-R RpoB substitutions (odds ratio (OR) = 8.69; 95% confidence interval (CI) = 2.95–30.84; $P < 0.001$) and DAP-R VREfm (OR = 6.47; 95% CI = 2.34–20.80; $P < 0.001$) (Supplementary Table 4a,b). Given that almost all patients who received rifaximin had underlying chronic liver disease (with hepatic encephalopathy being the predominant indication for rifaximin prescribing in Australia), we assessed the association between rifaximin and DAP resistance first within the subgroup of patients with liver disease ($n = 127$) (Supplementary Table 5a–c) and, second, in an independent cohort of patients without liver disease who had received rifaximin ($n = 57$) as antimicrobial prophylaxis after haematopoietic stem cell transplantation (HSCT) in Germany (Supplementary Table 6a–c). The association between rifaximin exposure and DAP-R RpoB substitutions was again identified in both patient groups—(1) patients with chronic liver disease ($P = 0.001$); and (2) HSCT patients without liver disease ($P < 0.001$) (Extended Data Fig. 4b and Supplementary Tables 5c and 6c). Among patients with liver disease colonized with VREfm, recent rifaximin was an independent predictor of DAP-R VREfm (OR = 4.37; 95% CI = 1.70–12.84; $P = 0.004$). We conducted other sensitivity analyses to verify the robustness of these associations and assess for other confounders, including a subgroup analysis that excluded patients who received rifaximin from the analysis (Supplementary Table 7), but these did not identify any other associations between DAP resistance and underlying disease or antibiotic exposure.

Six patients from the control group carried DAP-R VREfm—three (50%) of these had isolates with no mutations in *rpoB*, suggesting an alternative mechanism for resistance, while the remaining three patients had previously been admitted to the liver ward for inpatient care, suggesting that they may have acquired DAP-R VREfm through healthcare-associated transmission.

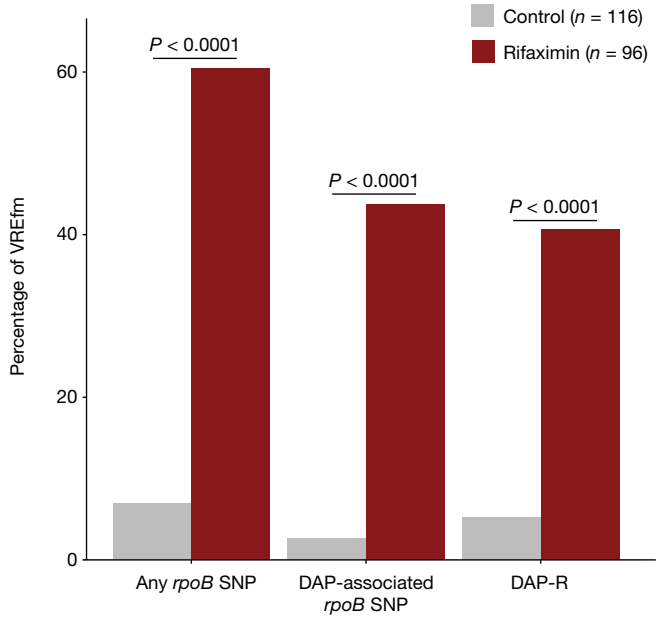

Fig. 3 | Rifaximin use is linked to DAP-R VREfm carriage. Summary of the percentage of VREfm with any *rpoB* SNP, DAP-associated *rpoB* SNP (S491F, G482D and H486Y) or DAP-R in patients in the control ($n = 116$) or rifaximin ($n = 96$) groups. Data were analysed using one-sided Fisher's exact tests. Exact *P* values were as follows: $P < 2.2 \times 10^{-16}$ (any *rpoB* SNP); $P = 3.044 \times 10^{-14}$ (DAP-associated *rpoB* SNP) and $P = 1.463 \times 10^{-10}$ (DAP-R).

While only one representative VREfm isolate from each patient was included in the above analysis, the de novo emergence of DAP-R VREfm carrying the G482D RpoB substitution was observed in one patient from whom multiple isolates had been collected during rifaximin therapy, consistent with rifaximin exposure driving the de novo emergence of DAP-R VREfm.

These data showed a strong clinical association between recent rifaximin exposure and patient gastrointestinal carriage of VREfm with DAP-resistance-associated RpoB substitutions, suggesting that exposure to rifaximin drives DAP-R VREfm.

Rifaximin use leads to de novo DAP-R VREfm

We used a mouse VREfm gastrointestinal colonization model to test whether rifaximin exposure caused de novo emergence of *rpoB* mutations that confer cross-resistance to DAP. Mice were colonized with a DAP-S (MIC 2 mg l^{-1}) clinical VREfm ST796 isolate (Aus0233) containing a WT *rpoB* allele before being administered a human-equivalent dose of either rifaximin, rifampicin, DAP or vehicle (Extended Data Fig. 5a,b). Rifampicin was chosen as a comparison as it is a rifamycin that is used in clinical practice. After 7 days of rifamycin treatment, we observed rifamycin-resistant VREfm in significantly more mice receiving rifampicin (80% of mice) or rifaximin (90% of mice) than in mice that received DAP (0% of mice) ($P < 0.0001$ and $P < 0.0001$; unpaired *t*-test) or vehicle (0% of mice) ($P < 0.0001$ and $P < 0.0001$; unpaired *t*-tests) (Extended Data Fig. 5c).

For each mouse, we then determined the percentage of individual VREfm isolates that were rifamycin resistant or DAP-R. There were significantly more rifamycin-resistant VREfm isolated from mice receiving rifaximin or rifampicin than mice receiving the vehicle control ($P < 0.0001$ and $P < 0.0001$; unpaired *t*-test) or DAP ($P < 0.001$ and $P < 0.001$; unpaired *t*-tests) (Extended Data Fig. 5d). Similarly, there were significantly more DAP-R VREfm in mice receiving rifaximin or rifampicin than in mice receiving the vehicle control ($P < 0.05$ and $P < 0.05$; unpaired *t*-tests) or DAP ($P < 0.05$ and $P < 0.05$; unpaired *t*-tests) (Fig. 4a,b). DAP-R VREfm accounted for between 0% and 41% of the gastrointestinal VREfm population in mice given rifaximin and between 0% and 36% in mice given rifampicin, demonstrating conclusively that rifamycin administration drives the emergence of VREfm with resistance to rifamycins and cross-resistance to DAP.

We next performed whole-genome sequencing (WGS) on 150 randomly selected VREfm isolates from each group (rifaximin or rifampicin; $n = 300$ total) to identify all of the mutations present in the rifamycin-resistant isolates. This collection consisted of 100 rifaximin- or rifampicin-resistant isolates taken after the last day of treatment and 50 isolates from each group collected before rifamycin administration. No substitutions in RpoB were identified in any *E. faecium* isolate taken before rifaximin or rifampicin exposure. However, after exposure, VREfm carrying mutations within *rpoB* were commonly identified. The S491F substitution was most prevalent ($n = 53$ (rifaximin) and $n = 63$ (rifampicin)), with all isolates carrying this substitution being DAP-R (Fig. 4c). H486Y was the second most common RpoB substitution identified ($n = 12$ (rifaximin) and $n = 28$ (rifampicin)), with all isolates again being DAP-R. The G482D substitution was the third most common RpoB substitution ($n = 15$ (rifaximin) and $n = 6$ (rifampicin)), with 19 isolates DAP-R. Other RpoB substitutions, including V135F, L471V, Q473L and H486R, were identified; however, all of the VREfm isolates carrying these substitutions were DAP-S. Importantly, the proportions of each RpoB substitution observed in VREfm collected from the gastrointestinal tract of mice administered rifamycin closely matched the proportions of each mutation observed in our collection of human clinical VREfm isolates, with the S491F substitution most identified, followed by H486Y and then G482D. These mouse model data strongly suggest that exposure to rifaximin is driving the de novo emergence of DAP resistance in colonizing strains of *E. faecium* in humans.

rpoB mutations upregulate the *prd* locus

We next used a multiomics approach to understand how amino acid substitutions in the β subunit of the bacterial RNA polymerase (RpoB) cause resistance to DAP, a cell membrane active antibiotic. We first compared the lipidomes of the three isogenic DAP-R RpoB mutants (G482D, H486Y or S491F) to that of WT VREfm. We also included an isogenic RpoB mutant that did not confer resistance to DAP (Q473L; DAP MIC 2 mg l^{-1}). Principal component analysis (PCA) of lipid species detected clearly separated the DAP-R RpoB mutants from the WT and DAP-S Q473L strain, indicating distinct lipid profiles (Fig. 5a). While the same classes of lipid species were observed in the WT and DAP-R RpoB mutants, there were significant reductions in anionic cardiolipins (CLs) and phosphatidylglycerols (PGs), as well as an increase in digalactosyldiacylglycerols (DGDGs) and cationic lysyl-PGs (Lys-PGs) in the RpoB mutants (Extended Data Fig. 6a–d). CL, PG, DGDG and Lys-PG profiles returned to WT when each of the three RpoB mutations was reverted to WT, demonstrating that the differences observed in the DAP-R strains were due to the RpoB substitutions (Supplementary Table 8).

Given the central role of RpoB in transcription, we posited that the lipidome differences of the DAP-R RpoB mutants were caused by alterations in gene expression. We modelled the RNA polymerase complex structure in *E. faecium* to assess the structural impact of changes imparted by Q473L, G482D, H486Y and S491F substitutions on transcription. All four substitutions were predicted to be present at the rifamycin active site and in direct interaction with nucleic acids at the transcription replication fork, with probable changes in stability or altered interactions with nucleic acid templates (Extended Data Fig. 6e). The S491F substitution defined changes to a bulkier hydrophobic side chain, with predicted mild reductions in protomer stability and affinities to rifampicin, other RNA polymerase subunits and nucleic acids within the replication fork. Thus, S491F is likely to directly impact the rate of transcription and rate of gene expression. Conversely, the G482D substitution resulted in the introduction of a bulkier negatively

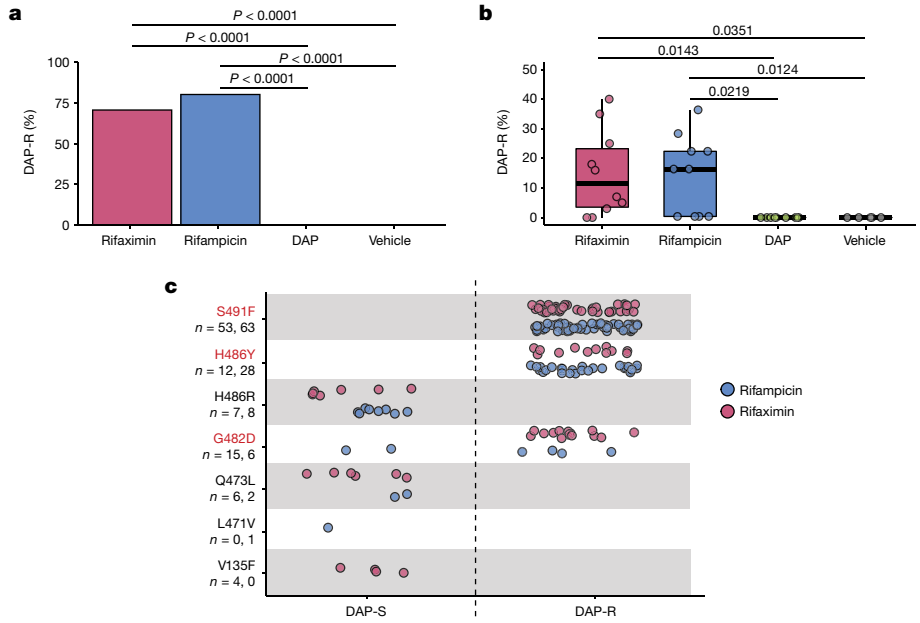

Fig. 4 | Rifaximin drives the emergence of DAP-R VREfm. a, The percentage of total mice ($n = 5$ mice for vehicle, $n = 10$ mice for rifampicin, $n = 10$ mice for rifaximin, $n = 10$ mice for DAP) with DAP-R VREfm strains. **b**, The percentage of VREfm from each mouse ($n = 50$ colonies from each individual mouse) that were resistant to DAP after 7 days of antibiotic treatment. The points represent the percentage of DAP-R VREfm from each individual mouse. The percentage was calculated from DAP MIC values (either resistant or susceptible) from the 50 VREfm colonies isolated from each mouse. For all box plots, the centre line shows the median, the box limits show the 25th and 75th percentiles, the upper and lower whiskers extend from the hinge to the largest and smallest values at most 1.5× interquartile range from the hinge. **c**, Overview of the RpoB substitutions identified in the rifampicin-resistant colonies. Each point represents a single VREfm isolate. Isolates are separated by each RpoB substitution and grouped into either DAP-S or DAP-R. The RpoB substitutions coloured in red had an association with DAP resistance. *n* values represent the number of isolates containing each mutation for rifaximin (left) and rifampicin (right). Data in **a** and **b** were analysed using two-sided unpaired *t*-tests (vehicle versus rifampicin or vehicle versus rifaximin and rifampicin verses DAP or rifaximin verses DAP). Exact *P* values are provided when the *P* value is above $P < 0.0001$.

charged side chain, which led to steric clashes and increased electrostatic potential of the RNA-binding cleft. The G482D substitution was predicted to have the largest detrimental effect on protein stability, which may reduce the amount of active RNA polymerase and gene expression. It was also predicted to increase nucleic acid binding affinity of the mutant complex, further reducing RNA polymerase activity and processing. Finally, the DAP-R substitution H486Y and DAP-S substitution Q473L were predicted to confer similar effects on protein stability, and rifampicin- and nucleic-acid-binding affinity. However, the H486Y substitution, but not the Q473 substitution, was predicted to increase RNA polymerase complex stability, reducing the dynamic flexibility required for enzyme activity, potentially leading to changes in gene expression. Overall, the DAP-R substitutions S491F, H486Y and G482D were all characterized by distinct interactions from the WT RNA polymerase while the DAP-S substitution Q473L retained the original WT interactions.

Given the predicted changes in RNA polymerase transcriptional activity, we used a combination of RNA sequencing (RNA-seq) and data-independent acquisition (DIA) based proteomics and identified 26 loci that were significantly differentially expressed in both RNA-seq and proteomics in all three DAP-R strains (G482D, H486Y and S491F), but not in the DAP-S strain (Q473L) or the WT VREfm (Extended Data Fig. 7a and Supplementary Table 9). No differences in expression (by transcriptomics or proteomics) of the *liaFSR*, *liaXYZ* or *yycFG* (*walKR*) regulons nor *cls* or *divIVA* genes were observed, indicating that the mechanism of RpoB-mediated DAP resistance was independent of previously described systems[7,8,16]. As compensatory *rpoC* mutations can alter the kinetic parameters of the RNA polymerase enzyme, we hypothesized that the number of dysregulated genes would decrease in the RpoBC double mutant (RpoB(S491F) and RpoC(T634K)) compared with the single RpoB(S491F) mutant, leaving genes that are possibly associated with DAP resistance. Indeed, only six loci were differentially expressed (on the basis of RNA-seq and proteomics) in the RpoBC mutant, compared with 44 loci identified in the single RpoB(S491F) mutant (Fig. 5b and Extended Data Fig. 7a). These included genes encoding a cold-shock protein (CspA, AGS75480 or EFAU233_01583), a hypothetical protein of unknown function (AGS75874 or EFAU233_01826), a potassium uptake transporter (K^+ transporter, AGS74117 or EFAU233_00176) and a DNA-binding transcriptional regulator of the PadR family in a putative operon with two hypothetical membrane proteins (AGS74325, AGS74326 and AGS74327, or EFAU233_00444, EFAU233_00445 and EFAU233_00446). All six of these loci were significantly upregulated (on the basis of RNA-seq and proteomics) in the three DAP-R RpoB mutants (G482D, H486Y and S491F), as well as in the RpoBC double mutant.

To understand their potential role in DAP resistance, each of these six genes were deleted from the VREfm Aus0233 WT and RpoB(S491F) mutant. The *dltC* gene, linked to DAP resistance in *Staphylococcus aureus*, was also deleted as it was differentially expressed in the G482D, H486Y and S491F strains, but not in the RpoBC double mutant. Of these 7 genes, only deletions of the PadR-family regulator (named here *prdR*, phenotypic resistance to DAP regulator) or the hypothetical membrane proteins (named here *prdA* and *prdB*) increased DAP susceptibility (by fourfold) in the WT or S491F backgrounds (Fig. 5c and Extended Data Fig. 7b). Similar fourfold increases in DAP susceptibility were observed when the *prdRAB* genes were deleted from the RpoB(G482D) or RpoB(H486Y) background (Fig. 5c).

Clinical paired VREfm isolates representative of the G482D, H486Y and S491F mutations were analysed using DIA proteomics to examine the abundance of PrdR, PrdA and PrdB in the cell. In DAP-R clinical strains carrying the S491F (ST1421 and ST203), G482D (ST80) or H486Y (ST203) mutations, the production of PrdRAB was significantly ($P < 0.05$) increased compared with DAP-S (WT *rpoB* allele) strains of the same ST (Extended Data Fig. 7c,d and Supplementary Table 9). The increased expression of PrdRAB in both genetically distinct clinical

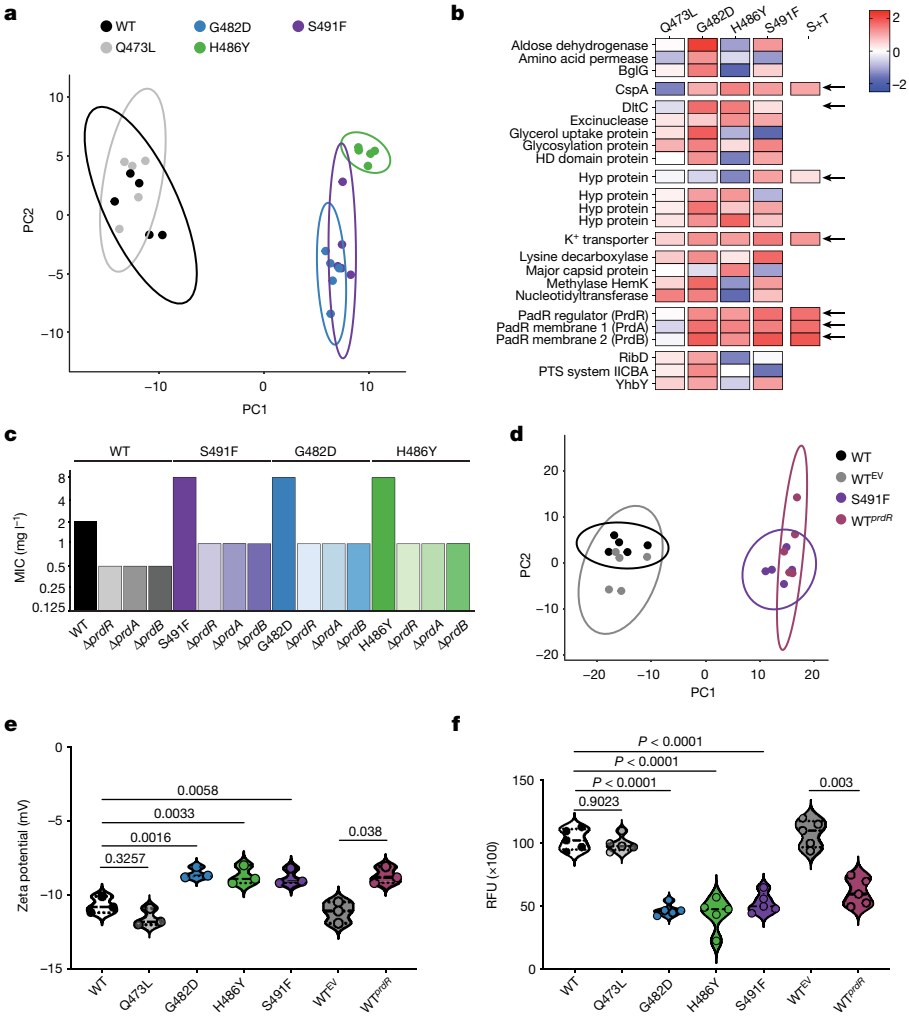

Fig. 5 | *rpoB* substitutions upregulate the *prdR* locus. a, PCA denoting segregation of the total lipid classes obtained for the WT and RpoB mutants. **b**, The 25 significantly differentially expressed loci identified in both RNA-seq and proteomics. The fold change value for RNA-seq is shown in the colour scale (log_2-transformed fold change). S+T, the double RpoB(S491F)/RpoC(T634K) mutant. **c**, Daptomycin susceptibility testing results for the WT and *rpoB* backgrounds (S491F, G482D or H486Y) with *prdR*, *prdA* or *prdB* deleted ($n = 3$). The MIC for each strain is shown without error bars as no variation between independent biological replicates was observed. **d**, PCA denoting the segregation of the total lipid classes obtained for the WT, S491F mutant, WT^{EV} and WT^{prdR}. **e**, The zeta potential (measured in mV). The points represent each biological replicate ($n = 3$), and the lines represent the median and interquartile range. Data were analysed using one-way analysis of variance (ANOVA) with correction for multiple testing using the Dunnett method, comparing WT versus RpoB mutant and WT^{EV} versus WT^{prdR}. **f**, Binding of BoDIPY–DAP, represented as relative fluorescence units (RFU). The points represent each biological replicate ($n = 5$) and the lines represent the median and interquartile range. Data were analysed using one-way ANOVA with correction for multiple testing using the Dunnett method, comparing WT versus RpoB mutant and WT^{EV} versus WT^{prdR}. Exact *P* values are provided when the *P* value is above $P < 0.0001$.

VREfm harbouring the G482D, H486Y or S491F mutations and in isogenic strains suggested that the *prdRAB* operon was responsible for RpoB-mediated DAP resistance.

PrdR overexpression leads to DAP-R VREfm

We hypothesized that the overexpression of the *prdRAB* operon in the RpoB mutants was leading to the observed changes in the cell membrane and resistance to DAP. Thus, an overexpression vector with the *prdR* gene, along with an empty vector (EV) control, were introduced separately into the WT VREfm. Plasmid-mediated overexpression of *prdR* increased the WT DAP MIC fourfold to 8 mg l^{-1}. Proteomic analysis (WT^{EV} versus WT^{prdR}) confirmed that PrdR was expressed at a similar level in the WT^{prdR} strain as in the RpoB mutants (2.5-fold and 2.2-fold in S491F, respectively) and PrdR specifically controlled the expression of the PrdAB membrane proteins (Extended Data Fig. 8a and Supplementary Table 9). PCA of the WT, WT^{EV}, WT^{prdR} and RpoB(S491F) lipidomes supported the overexpression of the *prdR* gene driving the changes in the lipid species, with the WT^{prdR} and RpoB(S491F) lipidomes clustering separately than the WT and WT^{EV} lipidomes (Fig. 5d and Supplementary Table 8). Reductions in the same anionic phospholipids (CL and PG) and increases in cationic Lys-PG species were observed in the WT^{prdR} strain at levels similar to those seen in the RpoB(S491F) mutant (Extended Data Fig. 8b–d). Lipidomic analyses of the previously described paired clinical isolates demonstrated the DAP-R clinical strains carrying RpoB mutations had similar significant differences in charged phospholipids (decreases in CL and PG, increases in Lys-PG), compared with DAP-S strains containing the WT *rpoB* allele (Extended Data Fig. 8e,f and Supplementary Table 8). These data indicated that overexpression of the *prdRAB* operon in DAP-R VREfm carrying RpoB mutations leads to changes in the abundance of charged lipid species in the cell membrane.

Given the decreases in anionic phospholipids (CL and PG) and increases in cationic phospholipids (Lys-PG), we tested whether strains with RpoB mutations have differences in overall cell membrane charge

and DAP binding. Both the DAP-R isogenic and clinical RpoB mutants (G482D, H486Y and S491F) had a significantly reduced negative charge associated with the cell membrane compared with their paired isolate (Fig. 5e and Extended Data Fig. 9a), respectively, and consequently bound to less fluorescent DAP (Fig. 5f and Extended Data Fig. 9c). Complementation of the RpoB mutations reversed cell membrane charge and DAP binding to WT levels (Extended Data Fig. 9b,d). No significant difference was observed in membrane charge or DAP binding for the DAP-S Q473L strain (Fig. 5e,f). Furthermore, the overexpression of the *prdR* gene resulted in a significantly reduced negative charge across the cell membrane compared with the WT^{EV} strain, with a similar charge to the DAP-R RpoB mutants (Fig. 5f). Moreover, binding of DAP was significantly decreased compared with the WT^{EV} strain (Fig. 5f). These experiments show that the increased expression of the *prdRAB* operon in VREfm carrying DAP-resistance-associated RpoB mutations leads to changes in the abundance of charged phospholipids and a decrease in the cell surface negative charge, which in turn reduces DAP binding to the cell membrane.

Discussion

Here we show that specific amino acid substitutions within the RRDR of RpoB (G482D, H486Y and S491F) lead to clinical DAP resistance in *E. faecium*. These mutations are spread in *E. faecium* populations worldwide, with their prevalence equal to well-characterized amino acid substitutions such as LiaFSR/LiaXYZ and Cls, that have been considered the dominant mechanisms of DAP resistance in VREfm[16,27,28]. Our multiomics analyses show that G482D, H486Y and S491F RpoB substitutions mediate DAP resistance through a conserved mechanism that is independent of previously described systems (Lia operons or Cls). We showed that each RpoB substitution leads to transcriptional dysregulation of a previously uncharacterized genetic locus, which we have named the phenotypic resistance to DAP, or *prd*, operon. Upregulation of the *prd* operon, which consists of a transcriptional regulator (PrdR) and two putative membrane proteins (PrdAB), leads to VREfm cell membrane remodelling and a decreased negative cell surface charge, that reduces DAP binding and, ultimately, renders VREfm resistant to DAP. The G482D, H486Y and S491F RpoB substitutions should therefore be considered to be clinically relevant and major mediators of DAP resistance in VREfm.

Exposure to rifamycin antimicrobials is well known to enrich for bacteria with RpoB substitutions[23,29,30]. Our data suggest that the clinical use of rifaximin is likely to be responsible for driving VREfm isolates with *rpoB* mutations that are resistant to not only rifamycins, but also DAP. Three lines of evidence support this hypothesis: Bayesian phylodynamic analyses show that the emergence of phylogenetically distinct VREfm lineages carrying the S491F substitution is temporally linked to the clinical approval of rifaximin in the early 2000s. Independent retrospective patient cohort studies demonstrated a robust association between recent rifaximin exposure and the carriage of DAP-R *E. faecium* with RpoB substitutions. Lastly, animal experiments demonstrated that administrating rifaximin to VREfm-colonized mice leads to the de novo emergence of DAP-R VREfm strains within the gastrointestinal tract, carrying the same substitutions within RRDR of RpoB as seen in patients.

Our study has potential limitations that warrant consideration when interpreting the results. Although our findings are substantiated by extensive orthogonal experimental evidence, the retrospective nature of our patient cohorts may introduce biases typical of such studies. These include selection and information biases, potentially arising from incomplete or imprecise patient medical records, such as antibiotic exposure history and underlying comorbidities. We implemented stringent genomic screening criteria to exclude clustered VREfm isolates from our cohort studies. However, possible undetected transmission events within the healthcare setting probably impact the assumption of independence in our logistic regression analyses, resulting in overly narrow confidence intervals. While our retrospective cohorts demonstrate a highly robust association between rifaximin use and DAP-R VREfm, these data alone cannot establish causation. Our conclusions are therefore based on the convergence of evidence from diverse experimental sources within our study, including phylodynamic modelling, controlled animal experimentation, extensive genomic epidemiology and independent retrospective patient cohorts. Future prospective multicentre studies would further validate our findings and address potential uncertainties in the reported effect size and confidence intervals.

Notwithstanding these limitations, we propose that patients with chronic liver disease receiving rifaximin are a primary source for the emergence and spread of DAP-R VREfm with *rpoB* mutations. Furthermore, our HSCT cohort analysis suggests the phenomenon extends beyond patients with liver disease, such that any patient colonized with VREfm and receiving rifaximin is at risk of DAP-R *E. faecium* emerging within the gut. These findings have important clinical implications. First, our data suggest that DAP should be avoided for empiric therapy of invasive VREfm infections in patients receiving or recently treated with rifaximin due to the higher risk of DAP resistance. Second, to preserve DAP efficacy, hospitals should consider maintaining isolation precautions for rifaximin-treated, VREfm-colonized patients, avoiding cohorting with other VREfm-colonized patients where possible. Lastly, while effective for hepatic encephalopathy prophylaxis, consideration should be given to keeping rifaximin as a second-line option behind other therapies for this indication, and its use for prophylaxis after HSCT should be reconsidered, given the propensity to induce *rpoB* mutations and subsequent DAP resistance.

Coordinated global efforts are underway to preserve last-resort antimicrobials through stringent stewardship protocols, limiting the use of these critically important medicines[31]. This strategy assumes that restricted antibiotic use correlates with reduced opportunities for pathogens to develop resistance. Our findings challenge this assumption, demonstrating that exposure to prophylactic rifaximin can lead to DAP-R VREfm emergence without direct DAP exposure.

Our data underscore the potential for unanticipated antimicrobial cross-resistance after the implementation of new treatment regimens, even those perceived to be low-risk and highlight the complex interplay between antimicrobial use and bacterial resistance mechanisms. The potential far-reaching impacts of seemingly benign antimicrobial regimens on AMR necessitates careful consideration, especially regarding the use of prophylactic antibiotics. Our research reinforces the need for judicious use of all antibiotics, and emphasizes the delicate balance required in managing AMR while meeting clinical needs.

Online content

Any methods, additional references, Nature Portfolio reporting summaries, source data, extended data, supplementary information, acknowledgements, peer review information; details of author contributions and competing interests; and statements of data and code availability are available at https://doi.org/10.1038/s41586-024-08095-4.

1. Murray, C. J. et al. Global burden of bacterial antimicrobial resistance in 2019: a systematic analysis. *Lancet* **399**, 629–655 (2022).
2. Cairns, K. A. et al. Therapeutics for vancomycin-resistant enterococcal bloodstream infections. *Clin. Microbiol. Rev.* **36**, e0005922 (2023).
3. Bass, N. M. et al. Rifaximin treatment in hepatic encephalopathy. *N. Engl. J. Med.* **362**, 1071–1081 (2010).
4. Arias, C. A. & Murray, B. E. The rise of the *Enterococcus*: beyond vancomycin resistance. *Nat. Rev. Microbiol.* **10**, 266–278 (2012).
5. Top, J., Willems, R. & Bonten, M. Emergence of CC17 *Enterococcus faecium*: from commensal to hospital-adapted pathogen. *FEMS Immunol. Med. Microbiol.* **52**, 297–308 (2008).
6. Arthur, M. & Courvalin, P. Genetics and mechanisms of glycopeptide resistance in enterococci. *Antimicrob. Agents Chemother.* **37**, 1563–1571 (1993).
7. Montero, C. I., Stock, F. & Murray, P. R. Mechanisms of resistance to daptomycin in *Enterococcus faecium*. *Antimicrob. Agents Chemother.* https://doi.org/10.1128/AAC.00774-07 (2008).

8. Diaz, L. et al. Whole-genome analyses of *Enterococcus faecium* isolates with diverse daptomycin MICs. *Antimicrob. Agents Chemother.* **58**, 4527–4534 (2014).
9. Lellek, H. et al. Emergence of daptomycin non-susceptibility in colonizing vancomycin-resistant *Enterococcus faecium* isolates during daptomycin therapy. *Int. J. Med. Microbiol.* **305**, 902–909 (2015).
10. Kelesidis, T., Tewhey, R. & Humphries, R. M. Evolution of high-level daptomycin resistance in *Enterococcus faecium* during daptomycin therapy is associated with limited mutations in the bacterial genome. *J. Antimicrob. Chemother.* **68**, 1926–1928 (2013).
11. Werth, B. J. et al. Defining daptomycin resistance prevention exposures in vancomycin-resistant *Enterococcus faecium* and *E. faecalis*. *Antimicrob. Agents Chemother.* **58**, 5253–5261 (2014).
12. Turner, A. M., Lee, J. Y. H., Gorrie, C. L., Howden, B. P. & Carter, G. P. Genomic insights into last-line antimicrobial resistance in multidrug-resistant *Staphylococcus* and vancomycin-resistant *Enterococcus*. *Front. Microbiol.* **12**, 637656 (2021).
13. Shayto, R. H., Abou Mrad, R. & Sharara, A. I. Use of rifaximin in gastrointestinal and liver diseases. *World J. Gastroenterol.* **22**, 6638–6651 (2016).
14. Sherry, N. L. et al. Pilot study of a combined genomic and epidemiologic surveillance program for hospital-acquired multidrug-resistant pathogens across multiple hospital networks in Australia. *Infect. Control Hosp. Epidemiol.* **42**, 573–581 (2021).
15. Gorrie, C. L. et al. Key parameters for genomics-based real-time detection and tracking of multidrug-resistant bacteria: a systematic analysis. *Lancet Microbe* **2**, e575–e583 (2021).
16. Miller, W. R., Bayer, A. S. & Arias, C. A. Mechanism of action and resistance to daptomycin in *Staphylococcus aureus* and *Enterococci*. *Cold Spring Harb. Perspect. Med.* **6**, a026997 (2016).
17. Goldstein, B. P. Resistance to rifampicin: a review. *J. Antibiot.* **67**, 625–630 (2014).
18. Rios, R. et al. Genomic epidemiology of vancomycin-resistant *Enterococcus faecium* (VREfm) in Latin America: revisiting the global VRE population structure. *Sci. Rep.* **10**, 5636 (2020).
19. Duchêne, S. et al. Genome-scale rates of evolutionary change in bacteria. *Microb. Genom.* **2**, e000094 (2016).
20. Lebreton, F. et al. Emergence of epidemic multidrug-resistant *Enterococcus faecium* from animal and commensal strains. *mBio* **4**, e00534-13 (2013).
21. Raven, K. E. et al. A decade of genomic history for healthcare-associated *Enterococcus faecium* in the United Kingdom and Ireland. *Genome Res.* **26**, 1388–1396 (2016).
22. Sensi, P. History of the development of rifampin. *Rev. Infect. Dis.* **5**, S402–S406 (1983).
23. Merker, M. et al. Transcontinental spread and evolution of *Mycobacterium tuberculosis* W148 European/Russian clade toward extensively drug resistant *Tuberculosis*. *Nat. Commun.* **13**, 5105 (2022).
24. Goel, A., Rahim, U., Nguyen, L. H., Stave, C. & Nguyen, M. H. Systematic review with meta-analysis: rifaximin for the prophylaxis of spontaneous bacterial peritonitis. *Aliment. Pharmacol. Ther.* **46**, 1029–1036 (2017).
25. Lee, R. A. et al. Daptomycin-resistant *Enterococcus Bacteremia* is associated with prior daptomycin use and increased mortality after liver transplantation. *Open Forum Infect. Dis.* **9**, ofab659 (2022).
26. Lee, R. S. et al. The changing landscape of vancomycin-resistant *Enterococcus faecium* in Australia: a population-level genomic study. *J. Antimicrob. Chemother.* **73**, 3268–3278 (2018).
27. Bender, J. K. et al. Update on prevalence and mechanisms of resistance to linezolid, tigecycline and daptomycin in enterococci in Europe: towards a common nomenclature. *Drug Resist. Updat.* **40**, 25–39 (2018).
28. Tran, T. T. et al. Whole-genome analysis of a daptomycin-susceptible *Enterococcus faecium* strain and its daptomycin-resistant variant arising during therapy. *Antimicrob. Agents Chemother.* **57**, 261–268 (2013).
29. Lee, J. Y. H. et al. Global spread of three multidrug-resistant lineages of *Staphylococcus epidermidis*. *Nat. Microbiol.* **3**, 1175–1185 (2018).
30. Guérillot, R. et al. Convergent evolution driven by rifampin exacerbates the global burden of drug-resistant *Staphylococcus aureus*. *mSphere* **3**, e00550-17 (2018).
31. Majumder, M. A. A. et al. Antimicrobial stewardship: fighting antimicrobial resistance and protecting global public health. *Infect. Drug Resist.* **13**, 4713–4738 (2020).

Methods

Media and reagents

E. faecium was routinely cultured at 37 °C in brain–heart infusion (BHI) broth (Becton Dickson) or BHI agar (BHIA), BHI solidified with 1.5% agar (Becton Dickson). For electroporation, *E. faecium* was cultured in BHI supplemented with 3% glycine and 200 mM sucrose (pH 7.0). *Escherichia coli* was cultured in Luria broth. Broth microdilution (BMD) MICs were performed in cation-adjusted Mueller Hinton with TES broth (CAMHBT) (Thermo Fisher Scientific). A concentration of 10 mg l^{-1} chloramphenicol (Sigma-Aldrich) was used for plasmid selection in *E. faecium* and *E. coli*. The following antibiotics were used at variable concentrations for susceptibility testing: rifampicin (Sigma-Aldrich), rifaximin (Sigma-Aldrich) and DAP (Cubicin).

Oligonucleotides were purchased from Integrated DNA Technologies and are listed in Supplementary Table 11. Plasmids were purified using the Monarch Plasmid Miniprep Kit (NEB). PCR products and gel extractions were purified using the Monarch DNA Gel Extraction Kit (NEB). Genomic DNA was purified using the Monarch Genomic DNA Purification Kit (NEB). Phusion and Phire DNA polymerase was purchased from NEB.

Bacterial isolates

A list of the bacterial strains used in this study is provided in Supplementary Table 10. Australian bacterial strains were collected across three data projects in the Microbiological Diagnostic Unit Public Health Laboratory (MDU PHL). Two unbiased cross-sectional surveys of VREfm were conducted between 10 November 2015 and 9 December 2015 ($n = 331$)[26] and between 1 November 2018 and 30 November 2018 ($n = 323$) in the state of Victoria (referred to as the 2015 and 2018 snapshot, respectively). During this period, all VREfm-positive isolates (including screening and clinical samples) collected by laboratories across the state were sent to the MDU PHL. Moreover, this project included *vanA*-VREfm collected from the Controlling Superbugs study[14,15], a 15-month (April 2017 to June 2017 and October 2017 to October 2018) prospective study including 8 hospital sites across 4 hospital networks, resulting in 346 VREfm isolates (308 patients) sent for WGS at MDU PHL. The VREfm were isolated from patient samples (including screening and clinical samples) routinely collected from hospital inpatients. For the 'historical *vanA*-VREfm,' every *vanA* isolate collected within MDU PHL was included. This resulted in an additional 229 isolates, sampled between 2003 and 2014. Collection of bacterial isolates for this study was approved by the Melbourne Health Human Research Ethics Committee (HREC), endorsed by the corresponding HREC at each participating site (HREC/13/MH/326) and the University of Melbourne Human Research Ethics Committee (22536). Approvals included a waiver of consent in accordance with the National Statement on Ethical Conduct in Human Research 2007 (Australia).

For publicly available isolates, our aim was to capture the diversity of *E. faecium* circulating globally by including isolates that formed part of several key studies involving hospital-associated VREfm (as of January 2021). To be included, isolates needed to have short-read data available, with geographical location (by country), year of collection and source (human or animal). Reads were included only if they had a sequencing depth of >50×. To capture the diversity of VREfm circulating in the USA, isolates from human sources were downloaded from the PathoSystems Resource Integration Center[32]. All isolates were confirmed to be *E. faecium* with the Kraken2 database (v.2.1.2)[33]. The final number of international isolates comprised those from Africa ($n = 8$), Asia ($n = 25$), Europe ($n = 2{,}941$), North America ($n = 424$) and South America ($n = 78$) (Supplementary Table 10).

Antibiotic susceptibility testing

Daptomycin susceptibility testing was performed using the BMD MIC method according to CLSI guidelines. In a 96-well plate, a twofold dilution series (from 32 to 0.5 mg l^{-1}) of DAP was made in 100 µl volumes of CAMHBT, additionally supplemented with 50 mg l^{-1} Ca^{2+}. An inoculum of 100 µl *E. faecium* broth culture adjusted to 1×10^6 colony-forming units (CFU) per ml in CAMHBT was then added to each well. After incubation for 24 h, the MIC was defined as the lowest antimicrobial concentration that inhibited visible growth. All assays were performed in biological triplicate, with the median MIC reported. In accordance with recent guidelines[34], isolates with a DAP MIC ≥ 8 mg l^{-1} were considered to be DAP-R. A DAP-sensitive strain (AUS0085)[35] and a DAP-R strain (DMG1700661)[36] were used as controls.

Rifampicin susceptibility testing was performed using the BMD method in CAMHBT. High-level rifampicin resistance was defined with a MIC > 32 mg l^{-1}. All susceptibility testing was performed in triplicate.

WGS analysis

Genomic DNA was extracted from a single colony using the JANUS automated workstation (PerkinElmer) and Chemagic magnetic bead technology (PerkinElmer). Genomic DNA libraries were prepared using the Nextera XT kit according to the manufacturer's instructions (Illumina). WGS was performed using the Illumina NextSeq platform, generating 150 bp paired-end reads. The short reads of isolates sequenced at MDU-PHL are available at the NCBI Sequence Read Archive (BioProject: PRJNA565795 (controlling superbugs), PRJNA433676 (2015 snapshot) and PRJNA856406 (2018 snapshot) and PRJNA856406 (historical *vanA* isolates)).

Phylogenetic analysis

De novo assemblies of the genomes were constructed using Spades[37] (v.3.13). In silico MLST was determined using the program mlst with the efaecium database[38] (https://github.com/tseemann/mlst). The 1,000 Australian genomes as well as the 4,705 Australian and international VREfm were mapped to the reference *E. faecium* genome AUS0085 isolated from a human bacteraemia infection in Victoria, Australia (NCBI: CP006620)[35] using snippy (https://github.com/tseemann/snippy) (v.4.4.5), applying a minfrac value of 10 and mincov value of 0.9. This reference was selected as it was a publicly available complete genome collected locally and DAP-S. A maximum-likelihood phylogenetic tree was inferred using IQ-TREE (v.2.1.2)[39] with a general time-reversible (GTR + G4) substitution model, including invariable sites as a constant pattern and 1,000 bootstrap replicates. Recombination masking was not performed for species maximum-likelihood trees due to the small size of the resulting core alignment. All trees were mid-point rooted and visualized in R (v.4.0.3; https://www.r-project.org/) using phangorn[40] (v.2.5.5), ape[41] (v.5.4), ggtree[42] (v.2.3.4) and ggplot (v.3.3.2).

The genome assemblies of all isolates were screened for acquired AMR determinants using abriTAMR (https://github.com/MDU-PHL/abritamr)[43].

GWAS analysis of DAP resistance

A GWAS approach was applied to identify genetic variants of DAP resistance in *E. faecium*. A genotype matrix of SNPs was constructed and used as input to homoplasyFinder[44] (v.0.0.0.9) to determine the consistency index at each locus and kept mutations that had an index of ≤0.5 (indicating at least two independent acquisitions across the phylogeny). We then ran GWAS using DAP resistance as a binary trait, where isolates were categorized as resistant if their DAP MIC was ≥8 mg l^{-1}. To correct for population structure, we used the factored spectrally transformed linear mixed models (FaST-LMM) implemented in pyseer[45] (v.1.3.6), which computes a kinship matrix based on the core genome SNPs as a random effect. *P* values were corrected for multiple-hypothesis testing using the Bonferroni correction method.

Competition assay

For competition assays, overnight cultures of WT and corresponding RpoB(S491F) or RpoB(S491F)/RpoC(T634K) mutants were diluted to

an optical density at 600 nm (OD_{600}) of 0.5 in BHI and equal volumes added to an overnight culture. Serial dilutions of each co-culture were performed at times 0 and 24 h on BHIA. Colonies were then replica plated onto BHIA and BHIA rifampicin 20 μg ml^{-1} to determine the proportion of WT to mutant.

cgMLST and clustering

cgMLST alleles for each isolate were defined using the public *E. faecium* cgMLST scheme[46] and chewBBACA (v2.0.16)[47], implemented locally in the COREugate pipeline (v.2.0.4) (https://github.com/kristyhoran/Coreugate). The pipeline determines the alleles of each core gene for every isolate as defined by the specific pathogen scheme. The *E. faecium* cgMLST scheme contains 1,423 genes. The number of allelic differences between each isolate within this core set of genes is then determined. The cgMLST clusters were determined using single linkage clustering and a pairwise allelic difference threshold of ≤250. This threshold was chosen as it maximized diversity within clusters, to improve temporal sampling depth, while still clustering based on maximum-likelihood tree structure.

Phylodynamic analysis of the emergence of the S491F(RpoB) mutation in VREfm lineages

To investigate the emergence of the S491F mutation in RpoB in three different lineages, as defined with cgMLST, we undertook further analysis on these clusters/lineages. From the species-level maximum-likelihood tree (Fig. 2c), three lineages/clusters were identifiable by cgMLST due to their size ($n > 50$) and presence of the S491F mutation. The three clusters were analysed independently, such that individual core-genome SNP alignments were generated, as this increased the length of the core alignment and number of sites considered. Snippy (https://github.com/tseemann/snippy) (v.4.4.5) was used to generate the alignments for each cluster to the corresponding reference genome (AUSMDU00004024 (CP027517.1) for cluster 1; AUSMDU00004055 (CP027506.1) for cluster 2; and AUSMDU00004142 (CP027501.1) for cluster 3). Each core alignment used a within 'cluster reference' (complete genome of the same cluster) to maximize core-SNP alignment length. The reference for each cluster was chosen as they were a locally collected closed genome. Recombination was removed from the final alignment using Gubbins[48] (v.2.4.1) to ensure that modelling was informed only by SNPs with tree-like evolution within the core genome. Maximum-likelihood trees for each of the three clusters were inferred from the core-SNP alignments (cluster 1, $n = 219$ taxa, 329 SNPs; cluster 2, $n = 85$ taxa, 541 SNPs; cluster 3, $n = 68$ taxa, 764 SNPs) with IQ-tree (v.2.1.2)[49] with a general time-reversible (GTR + G4) substitution model, including invariable sites as a constant pattern. Phylogenetic uncertainty was determined through 1,000 nonparametric bootstrap replicates.

To investigate temporal signal in the three clusters of VREfm genomes, we first used TempEst[50] (v.1.5). A root-to-tip regression analysis was performed on the root-to-tip branch distances within the three, cluster maximum-likelihood phylogenies as a function of year of collection, with the position of the root optimized according to the heuristic residual mean squared method.

The frequency of the emergence of the *rpoB* mutation in VREfm was inferred using a discrete trait model implemented in BEAST[51] (v.1.10.4). Under this model the SNP alignments are used to infer the evolutionary process (that is, phylogenetic tree, time and nucleotide substitution model parameters) for the three clusters. The alignments all shared the HKY substitution model and a constant-size coalescent population prior[19]. To avoid ascertainment bias due to using a SNP alignment, the number of constant sites was considered for the likelihood calculations. The molecular clock was a relaxed clock with an underlying lognormal distribution. The molecular clock was calibrated using isolation dates for each genome by year of collection and the mean clock rate is shared between all three alignments, but the model allows for the individual alignments to have different standard deviations of the log-normal distribution and also different branch rates. The mean molecular clock rate requires an explicit prior distribution, for which we used a Gamma distribution and a 0.95 quantile range of 4.9×10^{-6} and 1.1×10^{-4} substitutions per site per year. This informative prior means that it acts as an additional source of molecular clock calibration. The median substitution rate was similar for cluster 1 and cluster 2, at 9.7×10^{-7} (95% highest posterior density (HPD) 6.88×10^{-7}–1.24×10^{-6}) and 1.25×10^{-6} (95% HPD 7.68×10^{-7}–1.74×10^{-6}), respectively, but slightly faster for cluster 3 at 3.86×10^{-6} (95% HPD 2.23×10^{-6}–5.69×10^{-6}). Cluster 1 ($n = 219$) was inferred from a core alignment of 1,869,554 bp containing 329 SNP sites; cluster 2 ($n = 85$) was inferred from an alignment of 1,524,024 bp containing 541 SNP sites; and cluster 3 ($n = 68$) was inferred from an alignment of 1,860,780 bp containing 764 SNP sites.

The presence or absence of the S491F mutation in *rpoB* was used as a binary trait[52,53]. The trait model was shared between the three alignments, with the different Markov jumps and rewards (that is, changes of trait state and time spent in each state, respectively) recorded for each of the three alignments. The posterior distribution of model parameters was sampled using a Markov chain Monte Carlo of 100,000,000 iterations, sampling every 100,000 iterations. Two independent runs were run for the models. We assessed sufficient sampling from the stationary distributions by verifying the effective sample size of key parameters was around or above 200. The final MCC trees were visualized in R (v.4.0.3, https://www.r-project.org/) using ggtree[42] (v.2.3.4). The Markov jumps for the *rpoB* trait for each alignment were visualized in R (v4.0.3, https://www.r-project.org/).

Construction of isogenic mutants using allelic exchange and of pRAB11^{prdR}

The *rpoC*^{T634K}, *rpoB*^{G482D}, *rpoB*^{H486Y}, *rpoB*^{S491F}, *rpoB*^{Q473L}, ABC transporter (I274S), permease protein (G71S) or mannitol dehydrogenase (V288L) mutations were recombined into the chromosomal copy of each gene in ST796 VREfm (Ef_aus0233) by allelic exchange. Deletions of the CpsA, K^+ transporter, hypothetical protein, DltC or PrdRAB were also completed using allelic exchange. The region encompassing each gene was amplified by splice overlap extension (SOE)-PCR and recombined into pIMAY-Z[54] using the seamless ligation cloning extract (SLiCE)[55] method and transformed into *E. coli* IM08B[54]. The construct was transformed into electrocompetent VREfm[55], with allelic exchange performed as described previously[56]. Reversion of *rpoB*^{G482D}, *rpoB*^{H486Y} or *rpoB*^{S491F} mutations were completed using allelic exchange with a construct containing the respective wild-type allele. To construct a vector containing *prdR*, the vector pRAB11 was used. The *prdR* gene was amplified using Aus0233 genomic DNA. The *prdR* product was gel extracted, SLiCE cloned into amplified pRAB11, and transformed into IM08B, yielding pRAB11:*prdR*. The plasmid and EV were then electroporated into Aus0233.

Genome sequencing and analysis of all mutants was conducted as described, with resulting reads mapped to the Ef_aus0233 reference genome and mutations identified using Snippy (https://github.com/tseemann/snippy) (v.4.4.5).

VREfm in vivo gastrointestinal colonization experiments

Female C57BL/6 mice at 6–8 weeks of age were purchased from WEHI and maintained in a specific-pathogen-free facility at the Peter Doherty Institute for Infection and Immunity. The facility operates a 12 h–12 h light–dark cycle and maintains ambient temperature (18–23 °C) and humidity (40–60%). Animals were administered a standard mouse chow diet (Barastoc irradiated mouse cubes) and provided with water ad libitum. All animal handling and procedures were performed in a biosafety class 2 cabinet. Animal procedures were performed in compliance with the University of Melbourne guidelines and approved by The University of Melbourne Animal Ethics Committee (application IDs: 20094 and 28528). Animals were randomly assigned into cages on reception. After acclimatization, the cages were randomly assigned to treatment groups.

Experimental group sizes (treatment versus controls) were calculated using a power of 80%, an attrition rate of 15% and a type I error of 5%. The dose for each antibiotic was calculated using the US Food and Drug Administration (FDA) human conversion formula to ensure that each mouse was given a human-equivalent dose[57]. To establish gastrointestinal colonization of VREfm, mice were administered ceftriaxone (410 mg kg^{-1} day^{-1}; AFT Pharmaceuticals) through subcutaneous injection once daily for 4 days, followed by an antibiotic wean period of 24 h. Mice were then inoculated with 10^6 VREfm in 100 µl PBS by oral gavage. Then, 3 days after VREfm inoculation, single-housed mice were administered either rifaximin (113 mg kg^{-1} administered twice daily; Sigma-Aldrich), rifampicin (123 mg kg^{-1} administered once day; Sigma-Aldrich) or vehicle (Corn oil with 10% DMSO) through oral gavage; or DAP (50 mg kg^{-1} administered once daily; Cubicin) through subcutaneous injection (this results in similar exposure (AUC_{0-24}) to that observed in humans receiving 8 mg kg^{-1} of intravenous DAP[58]). The above antibiotic dosing protocol was followed for 7 days. Faecal samples were collected at specific timepoints throughout the experiment to determine VREfm gut colonization and for downstream rifamycin and DAP resistance analysis. Investigators were blinded to treatment groups with faecal samples de-identified on collection from individual mice before being resuspended in PBS to a normalized concentration (100 mg ml^{-1}). Serial dilutions of each de-identified faecal sample were performed, and the samples were plated onto Brilliance VRE agar (Thermo Fisher Scientific) for VREfm CFU enumeration.

For rifamycin and DAP analysis, VREfm colonies ($n = 50$ per de-identified faecal sample per mouse) from the Brilliance VRE agar plates were replica plated onto BHIA with and without rifampicin 20 µg ml^{-1} to determine the proportion of rifampicin-resistant VREfm in each mouse. Fifty colonies per mouse were then screened for DAP resistance, with a single colony being resuspended in PBS, then diluted 1/100 into CAMHBT containing 50 mg l^{-1} Ca^{2+} and 1/100 in CAMHBT containing 50 mg l^{-1} Ca^{2+} and 8 mg l^{-1} DAP. All suspected DAP-R colonies were confirmed using a DAP BMD MIC as before.

To determine which mutations were present in the rifamycin-resistant isolates, a random selection of 300 colonies, 150 from rifaximin-treated mice and 150 from rifampicin-treated mice (50 pre and 100 post for each treatment), were sampled for WGS as described above.

Analysis of patients receiving rifaximin for hepatic encephalopathy prophylaxis

To examine the potential association between rifaximin exposure and DAP-R VREfm, we analysed VREfm collected between 2014 and 2022 from a single quaternary hospital institution in Melbourne. In total, 225 patients were assessed for previous exposure to rifaximin, which was defined as at least a single dose administered before the collection date for the VREfm isolate and grouped into a rifaximin-exposed group and an unexposed control group. Only a single isolate was selected at random for testing and analysis from patients who had multiple samples with VREfm isolates. The VREfm isolates underwent WGS and DAP and rifampicin susceptibility testing as before. Patients with VREfm isolates that were assessed as genetically clustered with other VREfm isolates in the cohort and likely represented direct transmission were excluded. Genetic clustering was defined using an international standard SNP cut-off (7 SNPs)[59,60] using a split *k*-mer ($k = 15$) analysis (https://github.com/simonrharris/SKA) (v.1.0), a reference-free pairwise method that compares the entire genome (unlike traditional core-genome based comparisons). Medical records from patients were reviewed for comorbidity and antibiotic prescribing data. Potential associations were assessed through univariate analysis using Pearson's χ^2 tests or Fisher's exact tests for categorical data, and Student's *t*-tests (parametric) or Wilcoxon rank-sum tests (nonparametric) for continuous data. To determine predictors of DAP-R VREfm, multivariable logistic regression with backward stepwise elimination procedure was used, excluding variables with $P > 0.10$ and reincluding variables with $P < 0.05$. Exposure to rifampicin and DAP were forced into the models as variables a priori. A P value of <0.05 was considered to be statistically significant. Cases with missing data (for example, incomplete medical record data due to interhospital transfer) were excluded. Several sensitivity analyses were also performed to assess for independent associations after excluding potential confounders, including analysis with exclusion of variables with <10 outcomes, assessing associations with antimicrobial exposure separately from demographic and comorbidity data, and modifying the rifaximin exposure variable to include (1) any previous exposure to rifaximin (including both recent and distant exposure), and (2) any previous exposure to rifamycin antibiotics (including rifampicin, rifabutin and rifaximin). The genomic relationships of VREfm isolates were visualized in a maximum-likelihood phylogenetic tree as before, using a core-SNP alignment of 12,886 sites. The mutations in RpoB were determined using snippy (https://github.com/tseemann/snippy) (v.4.4.5) as described.

Data were obtained from medical records with approval from the Austin Health Human Research Ethics Committee (HREC/92971/Austin-2023), which included a waiver of consent in accordance with the National Statement on Ethical Conduct in Human Research 2023 (Australia).

Analysis of patients receiving rifaximin for HSCT prophylaxis

To examine the potential association between rifaximin exposure and the presence of DAP-associated *rpoB* substitutions in VREfm independent of underlying chronic liver disease, we analysed isolates collected from patients undergoing HSCT from a hospital institution in Regensburg, Germany. In this cohort, rifaximin is used for gut decontamination to reduce the risk of gastrointestinal graft-versus-host disease. Liver cirrhosis is a contraindication to HSCT. Notably, no patient received prophylactic DAP treatment, which is a major risk factor for DAP-R VREfm. There were 68 patients initially assessed for recent exposure to rifaximin, which was defined as at least a single dose administered within 90 days before the isolate collection date. Only a single isolate was retained for testing and analysis from patients who had multiple samples. In this instance, the isolate included was randomized. The isolates underwent WGS using ion-torrent next-generation sequencing technology (Thermo Fisher Scientific) and Nanopore sequencing (Oxford Nanopore). Patients with isolates that were assessed as genetically clustered with other isolates in the cohort and likely represented direct transmission were excluded (as above). Statistical and phylogenetic analyses were undertaken as described above.

Data were obtained from medical records with approval from the local ethics committee (ethical committee of the University of Regensburg, 21-2521–101). Stool samples were collected from patients after obtaining written informed consent, and the study was performed in accordance with the Declaration of Helsinki.

Lipidomic analyses

Cultures of VREfm ($n = 5$) were grown to mid-exponential phase ($OD_{600} = 0.6$) and washed in PBS. The protein content for each sample was measured using the Pierce BCA Protein Assay Kit (Thermo Fisher Scientific) and was normalized to 100 µg. Cells were lysed using the Bertin Precellys 24 homogenizer set at 6,000 rpm for 40 s and lipids were subjected to monophasic extraction as described previously[61]. Lipidomic samples were analysed using ultra-high-performance liquid chromatography (UHPLC) coupled to tandem mass spectrometry (MS/MS) using the Vanquish UHPLC system linked to an Orbitrap Fusion Lumos mass spectrometer (Thermo Fisher Scientific), with separate runs in positive- and negative-ion polarities. Solvent A comprised 60:40 (v:v) acetonitrile/water with 5 mM medronic acid and 10 mM ammonium acetate and solvent B comprised 90:10 (v:v) isopropanol:acetonitrile with 10 mM ammonium acetate. 10 µl of each sample was injected into the Acquity UPLC HSS T3 C18 column (1 × 150 mm, 1.8 µm; Waters) at 50 °C at a flow rate of 60 µl min^{-1} for 3 min using 3% solvent B. During

separation, the percentage of solvent B was increased from 3% to 70% in 5 min and from 70% to 99% in 16 min. Subsequently, the percentage of solvent B was maintained at 99% for 3 min. Finally, the percentage of solvent B was decreased to 3% in 0.1 min and maintained for 3.9 min.

All MS experiments were performed using an electrospray ionization source. The spray voltages were 3.5 kV in positive-ionization mode and 3.0 kV in negative-ionization mode. In both polarities, the flow rates of sheath, auxiliary and sweep gases were 25 and 5 and 0 arbitrary unit(s), respectively. The ion-transfer tube and vaporizer temperatures were maintained at 300 °C and 150 °C, respectively, and the ion funnel RF level was set at 50%. In the positive-ionization mode from 3 to 24 min, a top-speed data-dependent scan with a cycle time of 1 s was used. Within each cycle, full-scan MS spectra were acquired first in the Orbitrap at a mass resolving power of 120,000 (at m/z 200) across an m/z range of 300–2,000 using quadrupole isolation, an automatic gain control (AGC) target of 4×10^5 and a maximum injection time of 50 ms, followed by higher-energy collisional dissociation-MS/MS at a mass resolving power of 15,000 (at m/z 200), a normalized collision energy (NCE) of 27% in positive mode and 30% in negative mode, an m/z isolation window of 1, a maximum injection time of 35 ms and an AGC target of 5×10^4.

Identification and quantification of lipids and statistical analysis

LC–MS/MS data were searched using MS Dial v.4.90. The mass accuracy settings were 0.005 Da and 0.025 Da for MS1 and MS2. The minimum peak height was 50,000 and the mass slice width was 0.05 Da. The identification score cut-off was 80%. In positive-ionization mode, [M + H]+, [M + NH_4]+ and [M + H-H_2O]+ were selected as ion forms. In negative-ionization mode, [M-H]− and [M + CH_3COO]− were selected as ion forms. All lipid classes available were selected for the search. PC, Lys-PC, DG, TG, CE and SM were identified and quantified from positive-ionization mode while PE, LPE, PS, LPS, PG, LPG, PI, LPI, PA, LPA, Cer and CL were identified and quantified in negative-ionization mode. The retention-time tolerance for alignment was 0.1 min. Lipids with a maximum intensity of less than fivefold of average intensity in blank were removed. All other settings were set as the default. All lipid LC–MS features were manually inspected and reintegrated when needed. These four types of lipids, (1) with only sum composition except SM, (2) lipids identified due to peak tailing, (3) retention time outliner within each lipid class, (4) LPA and PA artefacts generated by in-source fragmentation of LPS and PS, were also removed. The shorthand notation used for lipid classification and structural representation follows the nomenclature proposed previously[62]. Relative quantification of the lipid species was achieved using the MS intensity of each lipid ion at apex of the LC peak and normalized to the protein quantity in each sample.

RNA-seq transcriptomics analysis

Cultures were grown to mid-exponential phase (OD_{600} = 0.6) and total RNA was extracted using the Direct-zol RNA Miniprep kit (Zymo Research) according to the manufacturer's instructions. Cells were lysed using the Bertin Precellys 24 homogenizer set at 6,000 rpm for 40 s. The samples were treated with TURBO DNase (Thermo Fisher Scientific) followed by clean-up using the RNA clean and concentrator kit (Zymo Research) according to the manufacturer's instructions. The absence of DNA contamination was checked by PCR and RNA integrity and purity was checked using the Bioanalyser RNA kit (Agilent). Five sequencing libraries from independent RNA extractions were made for each of the VREfm strains using the Stranded Total RNA with Ribo-Zero Plus (Illumina) kit and sequenced on a single lane of the Illumina NovaSeq 6000 platform. Raw paired-end reads were quality trimmed using TrimGalore (https://www.bioinformatics.babraham.ac.uk/projects/trim_galore/) (v.0.6.2). Bases with a quality score <20 and reads shorter than 50 bp after trimming were discarded. rRNA was removed by the BBDuk script in BBtools (https://sourceforge.net/projects/bbmap/) (v.39.01). The resulting reads were aligned to the Aus0233 reference genome by Bowtie2[63] (v.2.5.1) using the --no-mixed flag and read counts were generated using htseq-count[64] (v.0.12.4) using the options -r pos -t CDS -m union --nonunique none. Differentially expressed genes were detected using Degust (v.4.1.1). Genes with $\log_2$[fold change] > 1.5 and adjusted $P < 0.05$ were considered differentially expressed.

Proteomic analysis

Pelleted snap-frozen bacterial cells (OD_{600} = 0.6) were solubilized in 4% SDS, 100 mM Tris pH 8.5 by heating them for 10 min at 95 °C. The protein concentrations were assessed by a bicinchoninic acid protein assay (Thermo Fisher Scientific) and 100 µg of each biological replicate prepared for digestion using S-trap Mini Columns (Protifi) according to the manufacturer's instructions. In brief, the samples were reduced with 10 mM DTT for 10 min at 95 °C and then alkylated with 40 mM IAA in the dark for 1 h. The samples were acidified to 1.2% phosphoric acid and diluted with seven volumes of S-trap wash buffer (90% methanol, 100 mM tetraethylammonium bromide pH 7.1) before being loaded onto S-traps and washed three times with S-trap wash buffer. The samples were then digested with trypsin before being collected by centrifugation after the addition of 100 mM tetraethylammonium bromide, followed by 0.2% formic acid and then 0.2% formic acid/50% acetonitrile. The samples were dried and further cleaned up using C18 Stage[65,66] tips to ensure the removal of any particulate matter.

C18 enriched proteome samples were resuspended in 2% acetonitrile (aq) containing 0.01% trifluoroacetic acid (buffer A*) and separated using the Vanquish Neo UHPLC (Thermo Fisher Scientific) system with a single-column chromatography set up composed of a ACQUITY UPLC Peptide BEH C18 Column (300 Å, 1.7 µm, 1 mm × 100 mm, Waters) at a flow rate of 50 µl min^{-1}. Proteome samples were loaded directly on to the ACQUITY column with buffer A (0.1% formic acid, 2% DMSO) coupled directly to an Orbitrap 480 mass spectrometer (Thermo Fisher Scientific) and the buffer composition altered from 2% buffer B (0.1% formic acid, 77.9% acetonitrile, 2% DMSO) to 26% B over 70 min, then from 26% B to 99% B over 2 min and then was held at 99% B for 1.5 min. The mass spectrometer was operated in a data-independent mode automatically switching between the acquisition of a single Orbitrap MS scan (370–1,050 m/z, maximal injection time of 50 ms, an AGC set to a maximum of 300% and mass resolving power of 120,000 (at m/z 200) and the collection of 16.5 m/z DIA windows between 375 and 1,015 m/z (200–2,000 m/z, NCE 32%, maximal injection time of 54 ms, an AGC set to 1,000% and a mass resolving power of 30,000 (at m/z 200). Identification and label free quantification (LFQ) analysis were accomplished using Spectronaut (Biognosys) v.16 (16.0.220606.53000) using directDIA based analysis with minor modifications: protein LFQ method set to MaxLFQ, single hit proteins excluded and imputation disabled. Data were searched against the *E. faecium* Aus0004 proteome[35] (UniProt: UP000007591) with carbamidomethyl (C) allowed as a fixed modification and acetyl (protein N-term) as well as oxidation (M) allowed as variable modifications. Data outputs from Spectronaut were processed using Perseus (v.1.6.0.7)[67] with missing values imputed based on the total observed protein intensities with a range of 0.3 σ and a downshift of 1.8 σ. Statistical analysis was undertaken in Perseus using two-tailed unpaired t-tests and ANOVA. Proteins with $\log_2$[fold change] > 1 and adjusted $P < 0.05$ were considered to be differentially expressed.

Computational modelling

In predicting the potential effects of substitutions Q473L, G482D, H486Y and S491F, the full *E. faecium* DNA-dependent RNA polymerase was initially modelled using advanced homology modelling in Maestro (Schrodinger suite). BLAST-pdb was used to identify the *M. tuberculosis* homologue (PDB: 5UHC)[68] as the template, as it had the best sequence

identities across all RNA polymerase subunits. Modelling was performed based on the consensus between sequence alignments from MAFFT-DASH[69], T-COFFEE[70] and Clustal-W[71] (within Maestro), which were manually optimized to minimize sequence gaps. The final RNA polymerase model, bound to rifampicin and the DNA replication fork was next subjected to loop refinement and minimization, and iteratively assessed for model quality within Maestro.

The modelled structure was used as input within in silico biophysical predictors Dynamut2[72], mmCSM-lig (https://biosig.lab.uq.edu.au/mmcsm_lig/), mmCSM-NA[73] and mCSM-PPI2[73], which predicted the effects of mutations Q473L, G482D, H486Y and S491F on β-subunit stability, and affinities to rifampicin, nucleic acids within the replication fork, and other RNA polymerase subunits, respectively. During interpretation, all values were collectively considered to assess potential protein-level implications to wild-type function. In doing so, the affinity values for mutations located beyond 12 Å of the binding partner were presumed negligible.

Estimation of zeta potential

The zeta potential was measured on cells grown to exponential phase (OD_{600} = 0.6) and washed in PBS. The zeta potential measurements were performed in PBS to minimize the influence of pH. Each experiment was performed under identical experiment conditions (n = 5), 25 °C with 2 min of equilibration. The zeta potential was measured with a Zetasizer (Malvern).

Determination of cell-associated DAP with BoDipy labelling

BoDipy fluorescent dye (4,4-difluoro-1,3,5,7,8-pentamethyl-4-bora-3a,4a-diaza-*S*-indacene) (Invitrogen) was used to label DAP with minor modifications[74]. In brief, 50 µl DAP (50 mg ml^{-1}) was mixed with 100 µl BoDipy (10 mg ml^{-1}) and was made up to a final volume of 1 ml in 200 mM sodium bicarbonate (pH 8.5). The reaction was incubated for 1 h at 37 °C and unbound BoDipy was removed by dialysis at 4 °C using a Slide-A-Lyzer cassette (Thermo Fisher Scientific), with a 2.0 kDa cut-off according to the manufacturer's instructions. The antibiotic activity of BoDipy–DAP was confirmed by BMD (described above). To measure cell-associated DAP, cultures were grown to exponential phase (OD_{600} = 0.6) 50 mg l^{-1} $CaCl_2$. Each culture was incubated with BoDipy–DAP in darkness (10 min) and washed to remove unbound BoDipy–DAP. The amount of bound BoDipy–DAP was measured with excitation at 490 nm and emission at 528 nm using an Ensight microplate reader (PerkinElmer). Biological replicates (n = 5) were completed on separate days.

Data visualization and statistics

All figures were generated in R (v.4.0.3, https://www.r-project.org/) using tidyverse (v.1.3.1), patchwork (v.1.1.1), ggnewscale (v.0.4.5) and maps (v.3.4.2). Statistical analyses were performed using R (v.4.0.3, https://www.r-project.org/) and GraphPad Prism (v.9.3.1). Specific tests are provided together with each corresponding result in the text.

Reporting summary

Further information on research design is available in the Nature Portfolio Reporting Summary linked to this article.

Data availability

All data supporting the findings of this study are available within the Article and its Supplementary Information. The genomics data presented in the study are deposited under BioProject accessions PRJNA565795, PRJNA433676 and PRJNA856406. The MS proteomics data have been deposited in the Proteome Xchange Consortium via the PRIDE partner repository[75] under dataset identifiers PXD039832 and PXD039831. Correspondence and requests for materials should be addressed to G.P.C. or B.P.H. Source data are provided with this paper.

32. Snyder, E. E. et al. PATRIC: the VBI PathoSystems Resource Integration Center. *Nucleic Acids Res.* **35**, D401–D406 (2007).
33. Wood, D. E., Lu, J. & Langmead, B. Improved metagenomic analysis with Kraken 2. *Genome Biol.* **20**, 257 (2019).
34. Humphries, R. M. The new, new daptomycin breakpoint for *Enterococcus* spp. *J. Clin. Microbiol.* **57**, e00600-19 (2019).
35. Lam, M. M. et al. Comparative analysis of the complete genome of an epidemic hospital sequence type 203 clone of vancomycin-resistant *Enterococcus faecium*. *BMC Genom.* **14**, 595 (2013).
36. Li, L. et al. Daptomycin resistance occurs predominantly in vana-type vancomycin-resistant *Enterococcus faecium* in Australasia and is associated with heterogeneous and novel mutations. *Front. Microbiol.* **12**, 749935 (2021).
37. Bankevich, A. et al. SPAdes: a new genome assembly algorithm and its applications to single-cell sequencing. *J. Comput. Biol.* **19**, 455–477 (2012).
38. Homan, W. L. et al. Multilocus sequence typing scheme for *Enterococcus faecium*. *J. Clin. Microbiol.* **40**, 1963–1971 (2002).
39. Minh, B. Q. et al. IQ-TREE 2: new models and efficient methods for phylogenetic inference in the genomic era. *Mol. Biol. Evol.* **37**, 1530–1534 (2020).
40. Schliep, K. P. phangorn: phylogenetic analysis in R. *Bioinformatics* **27**, 592–593 (2011).
41. Paradis, E. & Schliep, K. ape 5.0: an environment for modern phylogenetics and evolutionary analyses in R. *Bioinformatics* **35**, 526–528 (2019).
42. Yu, G., Smith, D. K., Zhu, H., Guan, Y. & Lam, T. T.-Y. ggtree: an R package for visualization and annotation of phylogenetic trees with their covariates and other associated data. *Methods Ecol. Evol.* **8**, 28–36 (2017).
43. Sherry, N. L. et al. An ISO-certified genomics workflow for identification and surveillance of antimicrobial resistance. *Nat. Commun.* **14**, 60 (2023).
44. Crispell, J., Balaz, D. & Gordon, S. V. HomoplasyFinder: a simple tool to identify homoplasies on a phylogeny. *Microb. Genom.* **5**, e000245 (2019).
45. Lees, J. A., Galardini, M., Bentley, S. D., Weiser, J. N. & Corander, J. pyseer: a comprehensive tool for microbial pangenome-wide association studies. *Bioinformatics* **34**, 4310–4312 (2018).
46. de Been, M. et al. Core genome multilocus sequence typing scheme for high-resolution typing of *Enterococcus faecium*. *J. Clin. Microbiol.* **53**, 3788–3797 (2015).
47. Silva, M. et al. chewBBACA: a complete suite for gene-by-gene schema creation and strain identification. *Microb. Genom.* **4**, e000166 (2018).
48. Croucher, N. J. et al. Rapid phylogenetic analysis of large samples of recombinant bacterial whole genome sequences using Gubbins. *Nucleic Acids Res.* **43**, e15 (2015).
49. Nguyen, L.-T., Schmidt, H. A., von Haeseler, A. & Minh, B. Q. IQ-TREE: a fast and effective stochastic algorithm for estimating maximum-likelihood phylogenies. *Mol. Biol. Evol.* **32**, 268–274 (2015).
50. Rambaut, A., Lam, T. T., Max Carvalho, L. & Pybus, O. G. Exploring the temporal structure of heterochronous sequences using TempEst (formerly Path-O-Gen). *Virus Evol.* **2**, vew007 (2016).
51. Suchard, M. A. et al. Bayesian phylogenetic and phylodynamic data integration using BEAST 1.10. *Virus Evol.* **4**, vey016 (2018).
52. Minin, V. N. & Suchard, M. A. Counting labeled transitions in continuous-time Markov models of evolution. *J. Math. Biol.* **56**, 391–412 (2008).
53. Minin, V. N. & Suchard, M. A. Fast, accurate and simulation-free stochastic mapping. *Philos. Trans. R. Soc. B* **363**, 3985–3995 (2008).
54. Monk, I. R., Tree, J. J., Howden, B. P., Stinear, T. P. & Foster, T. J. Complete bypass of restriction systems for major *Staphylococcus aureus* lineages. *mBio* **6**, e00308-15 (2015).
55. Zhang, Y., Werling, U. & Edelmann, W. in *DNA Cloning and Assembly Methods* (eds Valla, S. & Lale, R.) 235–244 (Humana Press, 2014).
56. Pidot, S. J. et al. Increasing tolerance of hospital *Enterococcus faecium* to handwash alcohols. *Sci. Transl. Med.* **10**, eaar6115 (2018).
57. Nair, A. B. & Jacob, S. A simple practice guide for dose conversion between animals and human. *J. Basic Clin. Pharm.* **7**, 27–31 (2016).
58. Heine, H. S., Bassett, J., Miller, L., Purcell, B. K. & Byrne, W. R. Efficacy of daptomycin against *Bacillus anthracis* in a murine model of anthrax spore inhalation. *Antimicrob. Agents Chemother.* **54**, 4471–4473 (2010).
59. Higgs, C. et al. Optimising genomic approaches for identifying vancomycin-resistant *Enterococcus faecium* transmission in healthcare settings. *Nat. Commun.* **13**, 509 (2022).
60. Maechler, F. et al. Split *k*-mer analysis compared to cgMLST and SNP-based core genome analysis for detecting transmission of vancomycin-resistant enterococci: results from routine outbreak analyses across different hospitals and hospitals networks in Berlin, Germany. *Microb. Genom.* **9**, 000937 (2023).
61. Kralj, T. et al. Multi-omic analysis to characterize metabolic adaptation of the *E. coli* lipidome in response to environmental stress. *Metabolites* **12**, 171 (2022).
62. Liebisch, G. et al. Update on LIPID MAPS classification, nomenclature, and shorthand notation for MS-derived lipid structures. *J. Lipid Res.* **61**, 1539–1555 (2020).
63. Langmead, B. & Salzberg, S. L. Fast gapped-read alignment with Bowtie 2. *Nat. Methods* **9**, 357–359 (2012).
64. Anders, S., Pyl, P. T. & Huber, W. HTSeq—a Python framework to work with high-throughput sequencing data. *Bioinformatics* **31**, 166–169 (2015).
65. Rappsilber, J., Ishihama, Y. & Mann, M. Stop and go extraction tips for matrix-assisted laser desorption/ionization, nanoelectrospray, and lc/ms sample pretreatment in proteomics. *Anal. Chem.* **75**, 663–670 (2003).
66. Rappsilber, J., Mann, M. & Ishihama, Y. Protocol for micro-purification, enrichment, pre-fractionation and storage of peptides for proteomics using StageTips. *Nat. Protoc.* **2**, 1896–1906 (2007).
67. Cox, J. & Mann, M. MaxQuant enables high peptide identification rates, individualized p.p.b.-range mass accuracies and proteome-wide protein quantification. *Nat. Biotechnol.* **26**, 1367–1372 (2008).
68. Lin, W. et al. Structural basis of *Mycobacterium tuberculosis* transcription and transcription inhibition. *Mol. Cell* **66**, 169–179 (2017).
69. Rozewicki, J., Li, S., Amada, K. M., Standley, D. M. & Katoh, K. MAFFT-DASH: integrated protein sequence and structural alignment. *Nucleic Acids Res.* **47**, W5–W10 (2019).

70. Magis, C. et al. T-Coffee: tree-based consistency objective function for alignment evaluation. *Methods Mol. Biol.* **1079**, 117–129 (2014).
71. Higgins, D. G. & Sharp, P. M. CLUSTAL: a package for performing multiple sequence alignment on a microcomputer. *Gene* **73**, 237–244 (1988).
72. Rodrigues, C. H. M., Pires, D. E. V. & Ascher, D. B. DynaMut2: assessing changes in stability and flexibility upon single and multiple point missense mutations. *Protein Sci.* **30**, 60–69 (2021).
73. Nguyen, T. B., Myung, Y., de Sá, A. G. C., Pires, D. E. V. & Ascher, D. B. mmCSM-NA: accurately predicting effects of single and multiple mutations on protein-nucleic acid binding affinity. *NAR Genom. Bioinform.* **3**, lqab109 (2021).
74. Pader, V. et al. *Staphylococcus aureus* inactivates daptomycin by releasing membrane phospholipids. *Nat. Microbiol.* **2**, 16194 (2016).
75. Perez-Riverol, Y. et al. The PRIDE database resources in 2022: a hub for mass spectrometry-based proteomics evidences. *Nucleic Acids Res.* **50**, D543–D552 (2022).

Acknowledgements This work was supported by a National Health and Medical Research Council (NHMRC) of Australia Ideas grant (GNT1185213) to G.P.C., C.L.G. and I.R.M., and NHMRC project grant (GNT1160745) to B.P.H., T.P.S. and G.P.C. T.P.S. was supported by an NHMRC Investigator grant (GNT1194325). G.P.C. was supported by a University of Melbourne MDHS (Medicine, Dentistry and Health Sciences) mid-career seeding ideas grant and B.P.H. by an NHMRC Investigator Grant (GNT1196103). J.C.K. is supported by an NHMRC Early Career Fellowship (GNT1142613). A.M.T. and N.L.S. are supported by an Australian Government Research Training Program scholarship. D.J.I. is supported by an NHMRC Investigator Grant (GNT1195210). S.D. is supported by the Inception program (Investissement d'Avenir grant ANR-16-CONV-0005), an Investigator grant from the NHMRC (GNT2017284), and the Australian Research Council (FT220100629). The Controlling Superbugs study was supported by the Melbourne Genomics Health Alliance (funded by the State Government of Victoria, Department of Health and Human Services and the ten member organizations). N.E.S. is supported by an Australian Research Council Future Fellowship (FT200100270) and an ARC Discovery Project Grant (DP210100362). This study was also supported by Deutsche Forschungsgemeinschaft Projektnummer (324392634 – TRR 221 B13) to A.G., E.H. and D.W. We thank the staff at the Melbourne Mass Spectrometry and Proteomics Facility of The Bio21 Molecular Science and Biotechnology Institute for access to MS instrumentation and staff within the Microbiological Diagnostic Unit Public Health Laboratory for technical assistance with antimicrobial susceptibility testing and WGS.

Author contributions G.P.C., B.P.H. and C.L.G. conceived and planned the overall study design and supervised the project. A.M.T., L.L., J.Y.H.L. and G.P.C. performed all AST analyses. A.M.T. and I.R.M. designed plasmid constructs and generated all isogenic mutants. A.M.T., C.L.G. and A.H. analysed all WGS data and performed comparative genomic analyses. A.M.T., C.L.G., D.J.I. and S.D. performed phylodynamic (BEAST) analyses. G.P.C., L.L. and A.M.T. designed and performed all animal experimentation. J.C.K. led the collection and analysis of patient data from the Melbourne cohort, which was performed by J.C.K., S.V., N.I., B.C. and N.E.H. E.H. led the collection and analysis of patient data from the Regensburg cohort, which was performed by J.C.K., S.V., E.H., D.W. and A.G. G.P.C., L.L., N.E.S. and T.P.S. designed RNA-seq and DIA proteomics experiments, which were performed by A.M.T., with data then analysed by A.M.T., N.E.S., T.P.S. and C.J.W. Lipidomics experiments were designed by G.P.C., A.M.T., B.A.E. and G.E.R. and performed by A.M.T. and S.N., with data then analysed by A.M.T., G.E.R. and B.A.E. In vitro PrdRAB assays were performed by A.M.T. and L.K.S. In silico modelling of RNA polymerase was performed by S.P. and D.B.A. J.Y.H.L., T.S. and N.L.S. provided critical clinical and/or bioinformatics insights for the study. A.M.T., G.P.C. and C.L.G. co-wrote the manuscript with critical feedback from J.C.K., B.P.H. and T.P.S. and input from all of the authors.

Competing interests The authors declare no competing interests.

Additional information

Supplementary information The online version contains supplementary material available at https://doi.org/10.1038/s41586-024-08095-4.

Correspondence and requests for materials should be addressed to Benjamin P. Howden or Glen P. Carter.

Peer review information *Nature* thanks Cesar Arias, Judith Lok and the other, anonymous, reviewer(s) for their contribution to the peer review of this work. Peer reviewer reports are available.

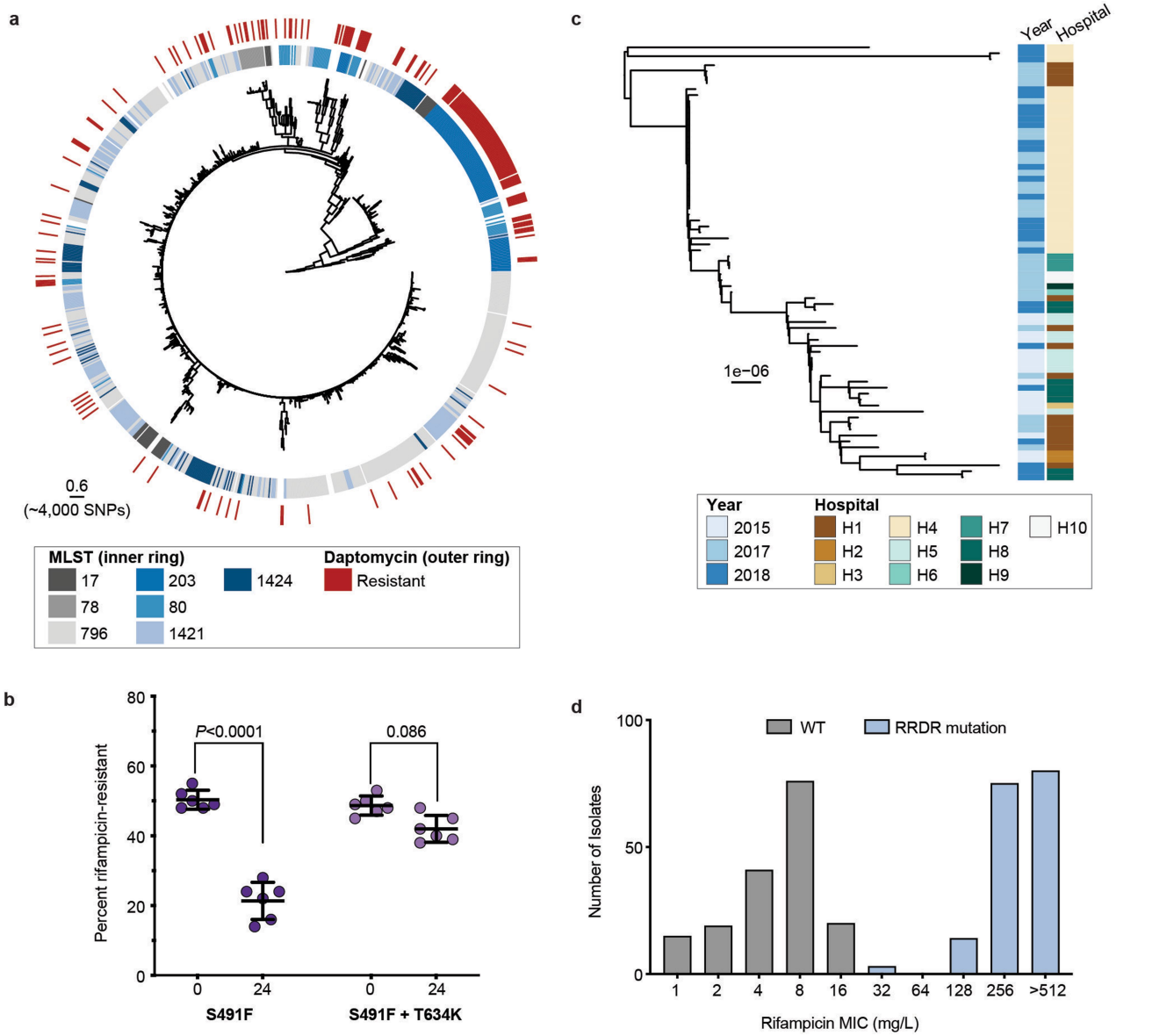

Extended Data Fig. 1 | Specific RpoB substitutions are associated with DAP resistance in VREfm. a. Maximum-likelihood core-SNP-based phylogeny of clinical VREfm (n = 1000) inferred from 6574 SNPs, demonstrating the interspersing of daptomycin resistance. Overlaid are the results of in silico MLST and daptomycin phenotypic testing. In the first heat map, ST is not shown for uncommon STs (n ≤ 5). The scale bar indicates number of nucleotide substitutions per site (top), with an approximation of SNP distance (in parentheses). ST=sequence type. SNP=single nucleotide polymorphism; MLST=multi-locus sequence type. **b**. Competition assays for the WT and RpoB S491F (dark purple) or WT and RpoB S491F/RpoC T634K (light purple) mutant pairs, with the percentage of rifampicin resistant (RIF^R) to rifampicin susceptible (RIF^S) isolates determined by plate count, shown on the y-axis. The x-axis denotes time in hours (either 0 or 24). Differences were assessed using two-way analysis of variance (ANOVA). All data points for independent biological replicates (n = 6) are displayed. Horizontal lines depict mean and error bars show the standard deviation. Exact *P* values are provided when the *P* value is above $P < 0.0001$. **c**. Maximum-likelihood core-SNP-based phylogeny of ST203, RpoB S491F VREfm (n = 80) inferred from 1960 SNPs, demonstrating the spread of isolates across different hospital networks. Overlaid are the year of isolation and hospital network for each isolate, represented as hospital 1 through 10 (H1-H10). The scale bar indicates number of nucleotide substitutions per site. **d**. Rifampicin susceptibility data for the clinical strains containing a mutation in the RpoB RRDR region (n = 169 isolates) versus a random selection of clinical strains containing a wild-type RRDR (n = 169 isolates). Bars represent the count of isolates containing each MIC. Three independent replicates were performed for each isolate. RRDR=rifampicin resistance determining region; MIC=minimum inhibitory concentration.

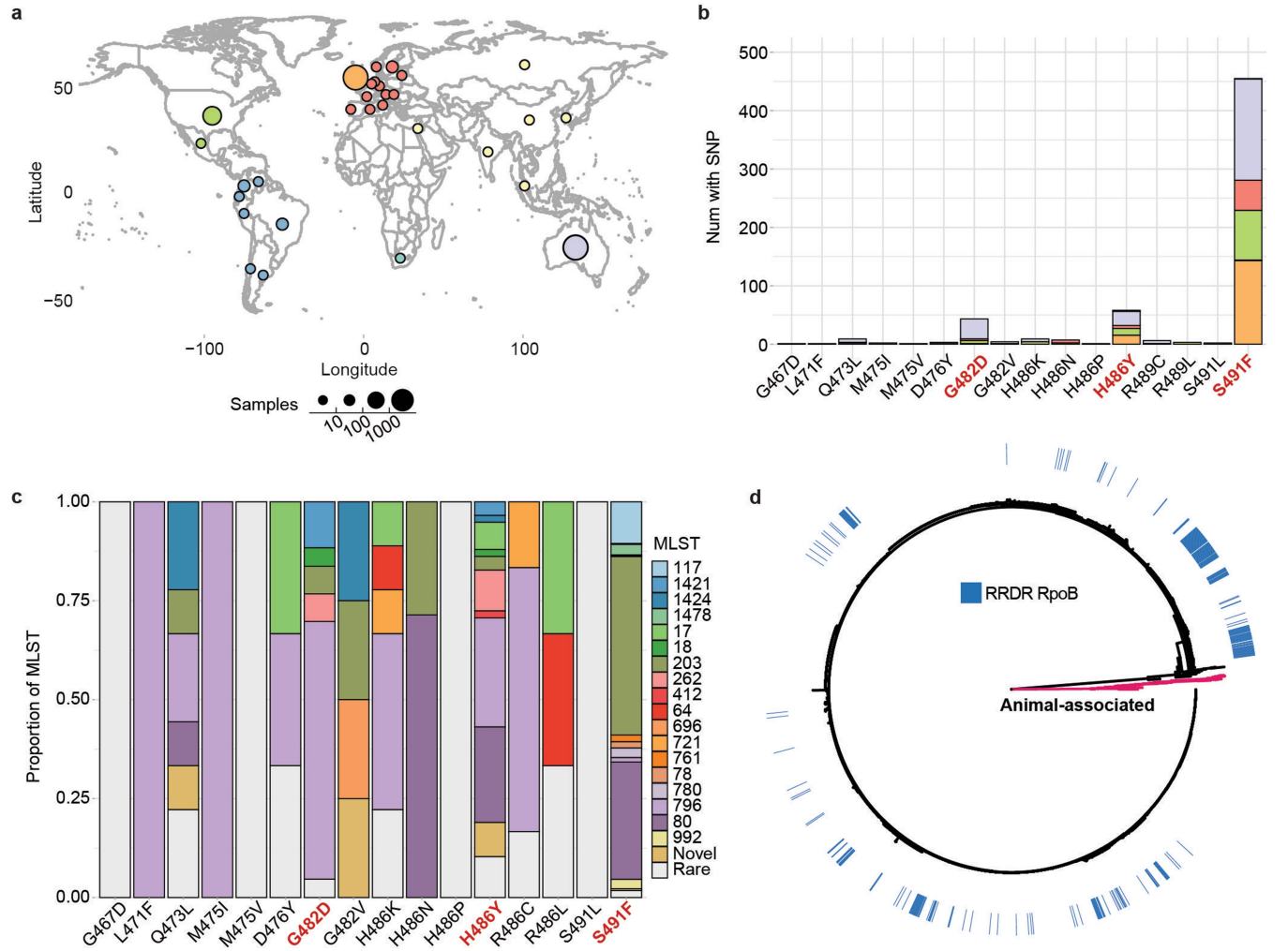

Extended Data Fig. 2 | DAP resistance RpoB substitutions are present globally. a. Map of 4,476 VREfm genomes included. Circle size corresponds to total number of genomes and colour corresponds to region of isolation. Country coordinates are the country centroid position. This map is derived from the public domain project Natural Earth and available from www.naturalearthdata.com ("world"). **b**. The frequency of RpoB substitutions within the rifampicin resistance determining region (RRDR) in 4,476 VREfm genomes, sampled from 43 MLSTs. Bars are coloured by the number of isolates from each region of isolation containing the mutation. The identified daptomycin resistance associated mutations are coloured in red. **c**. The frequency of various MLSTs identified in the 630 VREfm carrying RpoB mutations in the rifampicin resistance determining region (RRDR). The identified daptomycin resistance mutations are coloured in red. **d**. Maximum-likelihood core-SNP-based phylogeny of clinical (n = 4,378) and animal VREfm (n = 98) inferred from an alignment of 8,435 SNPs, demonstrating the presence of RRDR RpoB mutations in clinical VREfm isolates. Overlaid is a heatmap showing the presence of at least one substitution in the RRDR of RpoB. VREfm that were animal-associated are highlighted in pink.

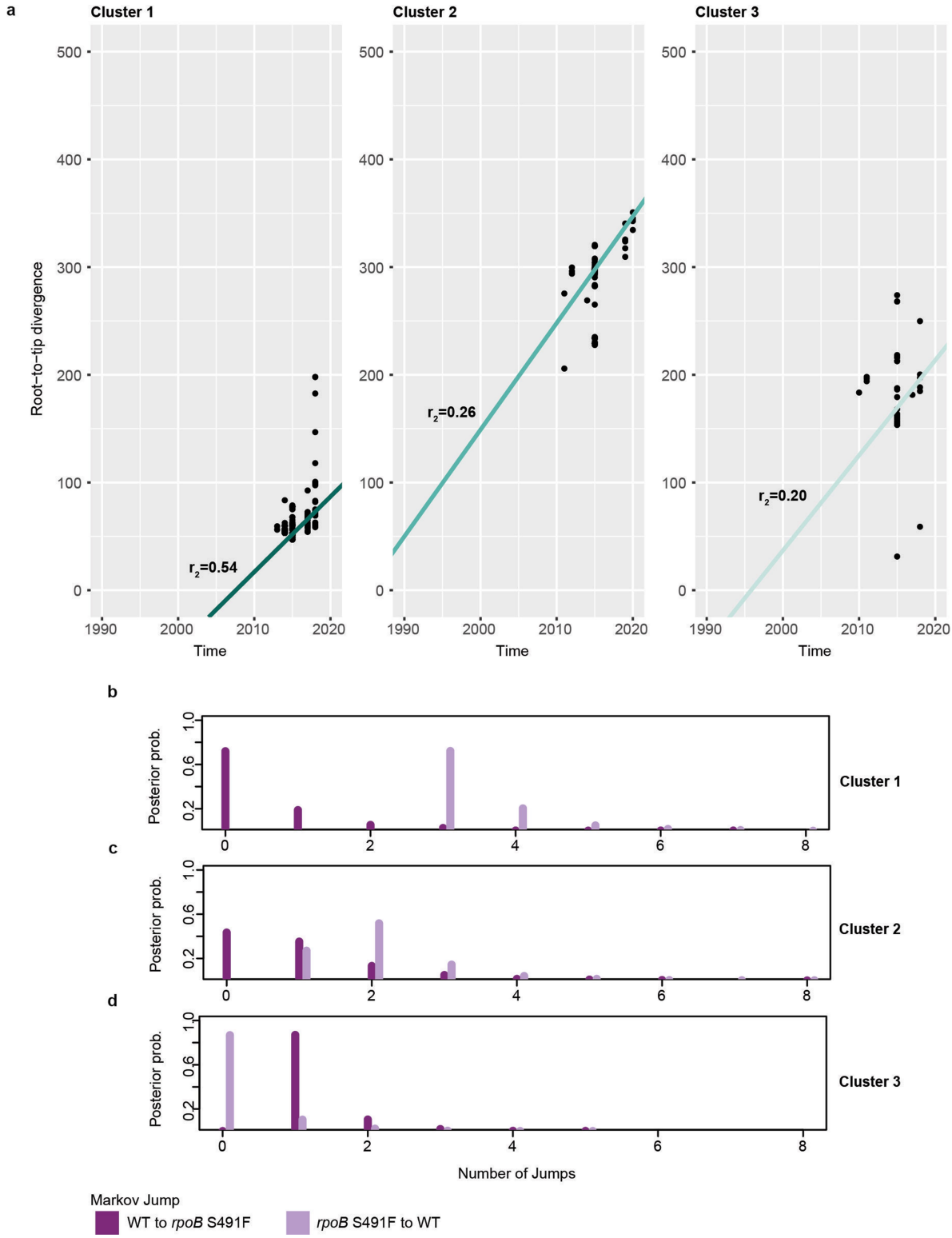

Extended Data Fig. 3 | The RpoB S491F substitution is maintained in the VREfm population. a. Linear regression of root-to-tip distance as a function of sampling time. The slope is a crude estimate of the substitution rate (substitution/site) for the recombination-free SNP alignment, with the x-intercept indicative of the age of the root node and the r^2 is a measure of clocklike behaviour. The x-axis is time (in years) and the y-axis displays the root-tip-divergence. The points represent an individual isolate in each cluster. **b-d.** Markov jump counts for the number of transitions between the binary trait of wild-type (WT) *rpoB* allele and RpoB S491F substitution. The number of Markov jumps for each cluster is shown on the x-axis, with the height of each bar representing the posterior probability for each individual jump.

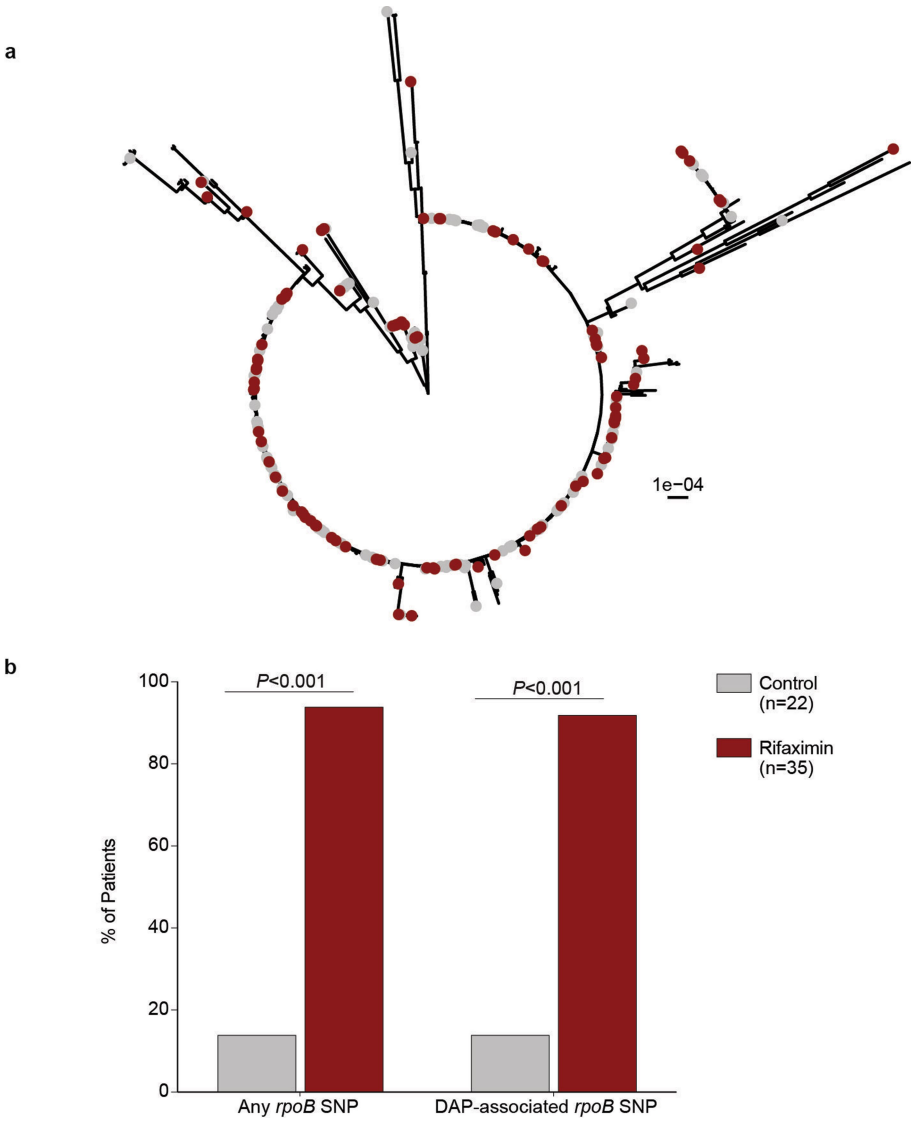

Extended Data Fig. 4 | Rifaximin prophylaxis is associated with DAP resistance in VREfm colonized patients. a. Maximum-likelihood, core-SNP-based phylogeny for VREfm inferred from 14,420 core-genome SNPs, demonstrating which isolates were from the "control" (n = 116) or "rifaximin" (n = 96) groups from the Melbourne cohort. The scale bar indicates number of nucleotide substitutions per site. **b**. Summary of the percentage of HSCT patients (Germany cohort; n = 22 control patients and n = 35 rifaximin patients) with a VREfm isolate with any *rpoB* SNP or daptomycin (DAP) associated *rpoB* SNP (G482D, H486Y, or S491F). Data was analysed using a Fisher's exact test (one-sided). The y-axis represents the number (shown as percent) of patients in the control or rifaximin group containing a *rpoB* mutation.

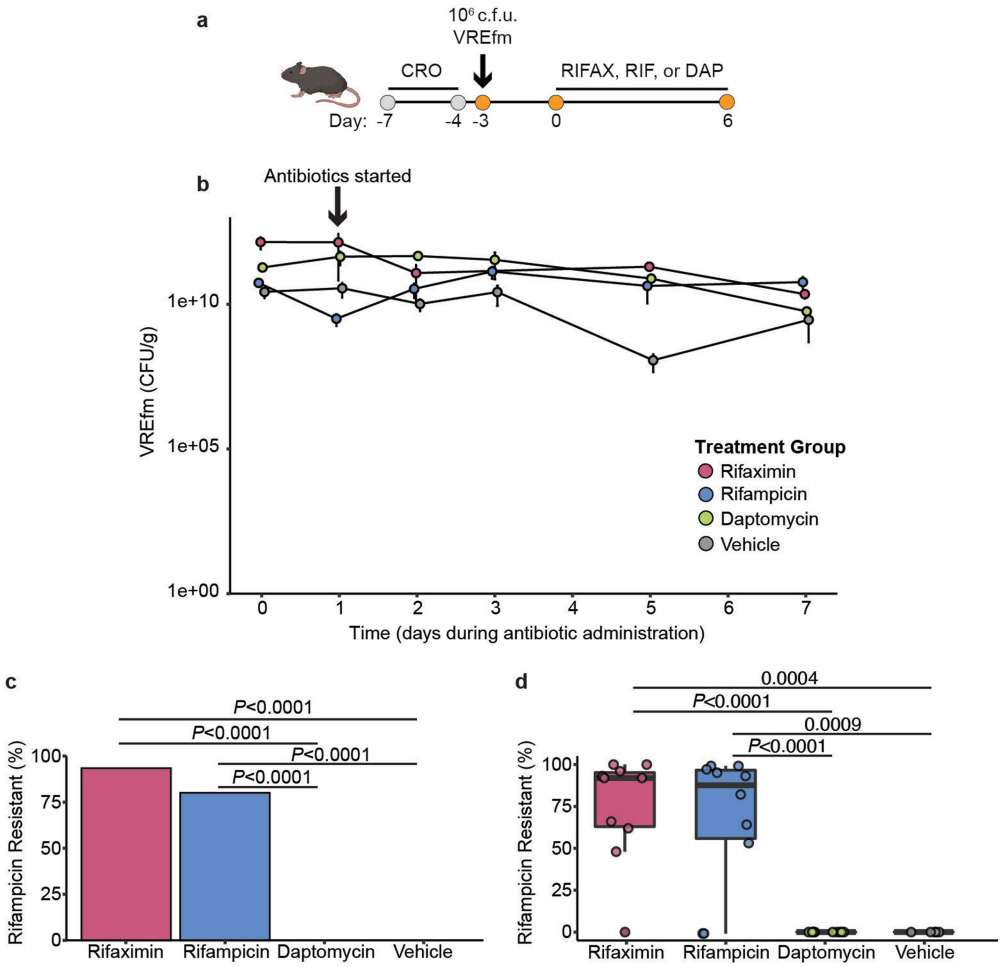

Extended Data Fig. 5 | Rifaximin drives daptomycin resistance in VREfm colonized mice. a. Timeline of the mouse experiment. VREfm-colonized mice (n = 5 independent mice for vehicle, n = 10 independent mice for rifampicin, n = 10 independent mice for rifaximin, n = 10 independent mice for daptomycin) received a human-equivalent dose of vehicle, rifampicin, or rifaximin (twice per day for rifaximin) for 7 days by oral gavage or subcutaneous injection with daptomycin for 7 days. CRO=ceftriaxone; DAP=daptomycin; RIFAX=rifaximin; RIF=rifampicin. Figure to scale. **b**. The colony forming units (CFU) for the duration of the mouse experiment. Each point represents the average VREfm CFU/g of faeces and error bars represent standard error of the mean. n = 5 independent mice for vehicle and n = 10 independent mice for DAP, RIF, and RIFAX. The x-axis is day of collection and y-axis is the CFU/g faeces of VREfm. **c**. Percentage of mice with rifampicin-resistant VREfm strains for each treatment group. **d**. Percentage of VREfm from each mouse (n = 50 colonies from each individual mouse) that were resistant to rifampicin after 7 days of antibiotic treatment. Points represent the percentage of rifampicin-resistant VREfm from each individual mouse. Percentage was calculated from rifampicin MIC values (either resistant or susceptible) from the 50 VREfm colonies isolated from each mouse. For all box plots, the lower and upper hinges depict the 25th and 75th percentiles. The upper and lower whiskers extend from the hinge to the largest and smallest values at most 1.5 × IQR from the hinge. The centre line in the box shows the median. Data in **c** and **d** were analysed using an unpaired *t*-test (two-sided) (vehicle versus rifampicin or vehicle versus rifaximin and rifampicin versus daptomycin or rifaximin versus daptomycin). Exact *P* values are provided when the *P* value is above $P < 0.0001$. The y-axes represent the percentage of rifampicin-resistant VREfm isolates.

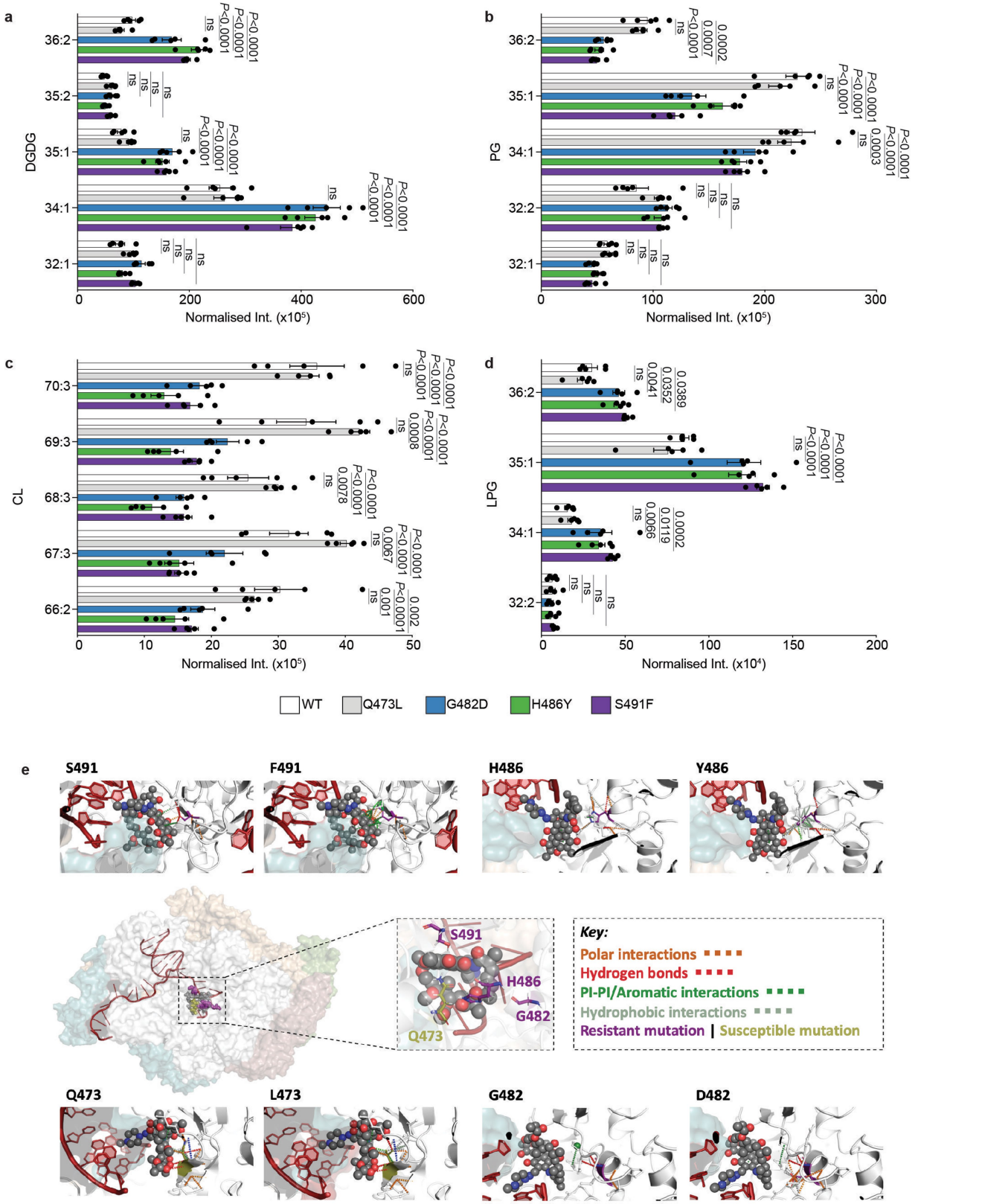

Extended Data Fig. 6 | Cell membrane lipid profile and molecular modelling of RpoB mutants. a-d. The main lipid species differentially produced by the WT and RpoB mutants shown as normalized abundance (intensity/total protein). Bars represent the median value and error bars represent the SEM. Each point represents an independent biological sample (n = 5). Data was analysed with a Two-way ANOVA (WT versus RpoB mutant) and *P* values were corrected for multiple testing using the Dunnett method. Exact *P* values are provided when the *P* value is above $P < 0.0001$; ns=not significant. The y-axis is the normalized intensity (Normalized Int.) for each lipid identified. **e.** Structural localization of missense *rpoB* mutations. All studied mutations were located within interaction proximity of the ligand rifampicin binding site (grey), and the nucleic acids of the replication fork (dark red).

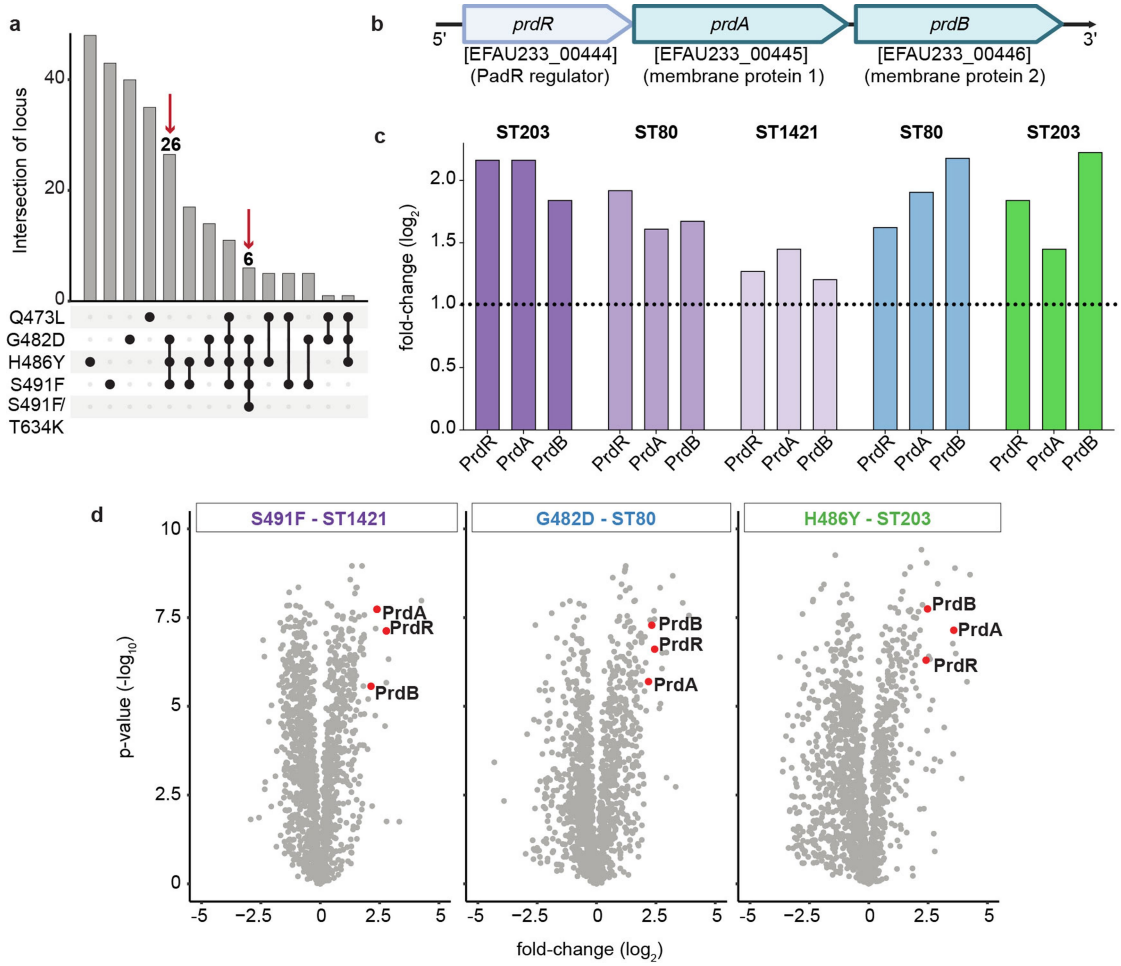

Extended Data Fig. 7 | PrdR is over-expressed in VREfm with RpoB substitutions. a. Intersection between RNAseq and proteomics analyses displayed as an UpSet plot (n = 5 independent biological replicates for RNAseq and n = 5 independent biological replicates for proteomics). The bar represents the count of each locus that was identified in each sample. RNA seq significance (FDR < 0.05, $log_2FC > 1$ or $log_2FC < -1$) and proteomics significance (adjusted p-value < 0.05, $log_2FC > 1$ or $log_2FC < -1$). **b.** Locus map of the *prdR* locus in the VREfm AUS0233 genome ([proteins] AGS74325, AGS74326, AGS74327 or EFAU233_00444, EFAU233_00445, EFAU233_00446). **c.** Proteomics comparing the abundance of the PrdRAB locus across five different clinical strain pairs (n = 5 independent biological replicates for each strain). Bars are the fold-change (log_2) from five independent biological replicates showing proteins with statistically significant (<0.05) *P*-values. The y-axis is the log_2 fold-change. Data was analysed using an unpaired *t*-test of daptomycin-susceptible clinical strain versus daptomycin-resistant clinical strain (with a RpoB mutation). **d**. Protein abundance changes of the clinical VREfm strain pairs (n = 5 independent biological replicates each isolate) containing mutations in RpoB from different genetic backgrounds, demonstrating the conserved upregulation of the PrdRAB operon. The x-axis is the log_2 fold-change and the y-axis is the $-log_{10}$ *P* value.

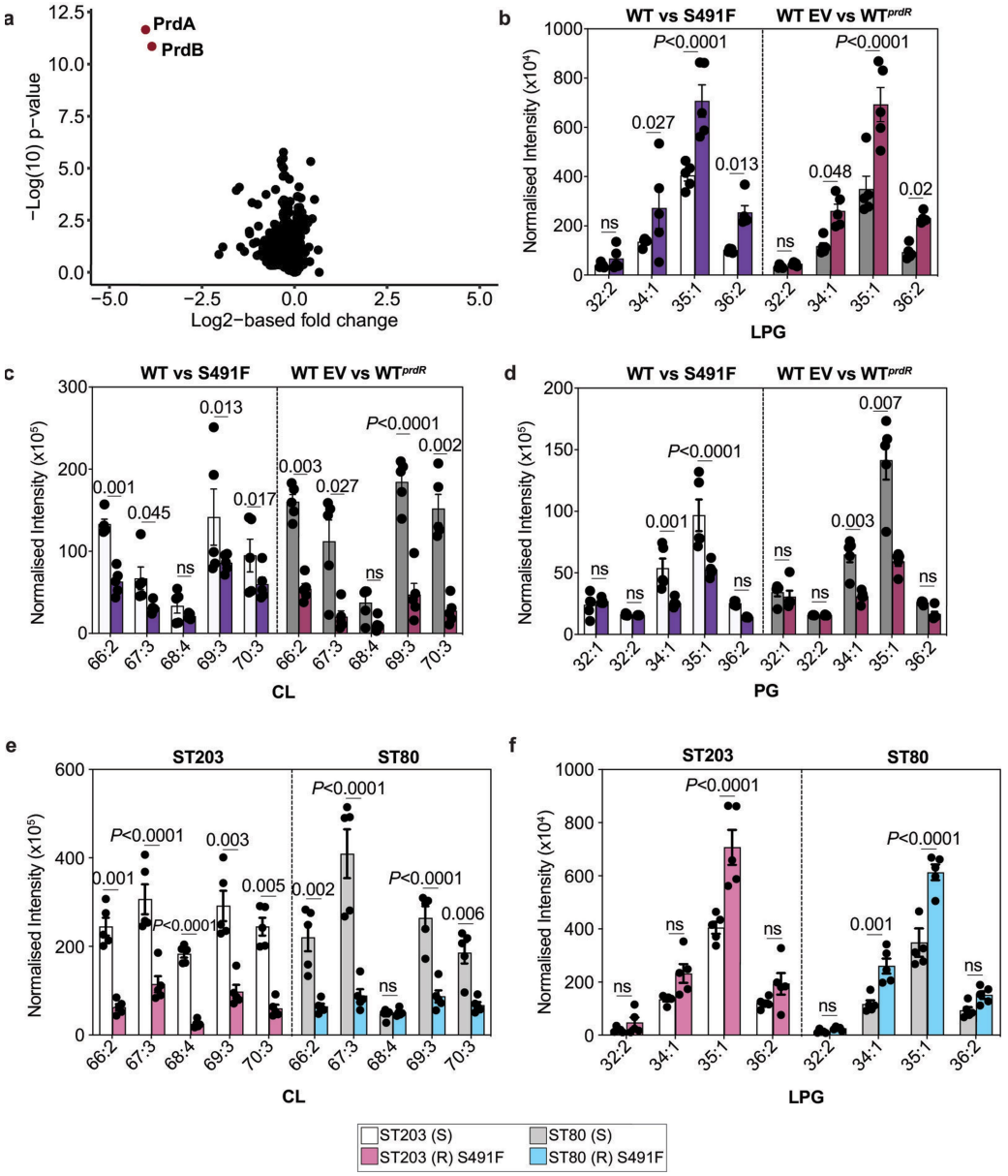

Extended Data Fig. 8 | PrdR over-expression changes the cell membrane lipid profile. a. Protein abundance changes for the *prdR* deletant mutant, compared to the WT strain, demonstrating the specificity of the regulator for the *prdAB* membrane proteins (n = 5 independent biological replicates for proteomics). The x-axis is the $\log_2$ fold-change and the y-axis is the $-\log_{10}$ *P* value. **b-d**. The lipid species differentially produced by the WT, S491F mutant, WT EV, and WT^{prdR} shown as normalized abundance (intensity/total protein). Bars represent the median value and error bars represent the SEM. Each point represents independent biological replicates (n = 5). Data was analysed with a Two-way ANOVA ((WT versus RpoB mutant and WT EV versus WT^{prdR}) and *P* values were corrected for multiple testing using the Dunnett method. Exact *P* values are provided when the *P* value is above $P < 0.0001$; ns=not significant. The y-axis is the normalized intensity (Normalized Int.) for each lipid identified. **e-f**. Lipid species differentially produced by the ST203 and ST80 RpoB S491F clinical strain pairs, shown as normalized abundance (intensity/total protein). Bars represent the median value and error bars represent the SEM. Each point represents independent biological replicates (n = 5). Data was analysed with a Two-way ANOVA (DAP-S versus DAP-R) and *P* values were corrected for multiple testing using the Dunnett method. Lipid species with a significant difference are denoted. The y-axis is the normalized intensity (Normalized Int.) for each lipid identified.

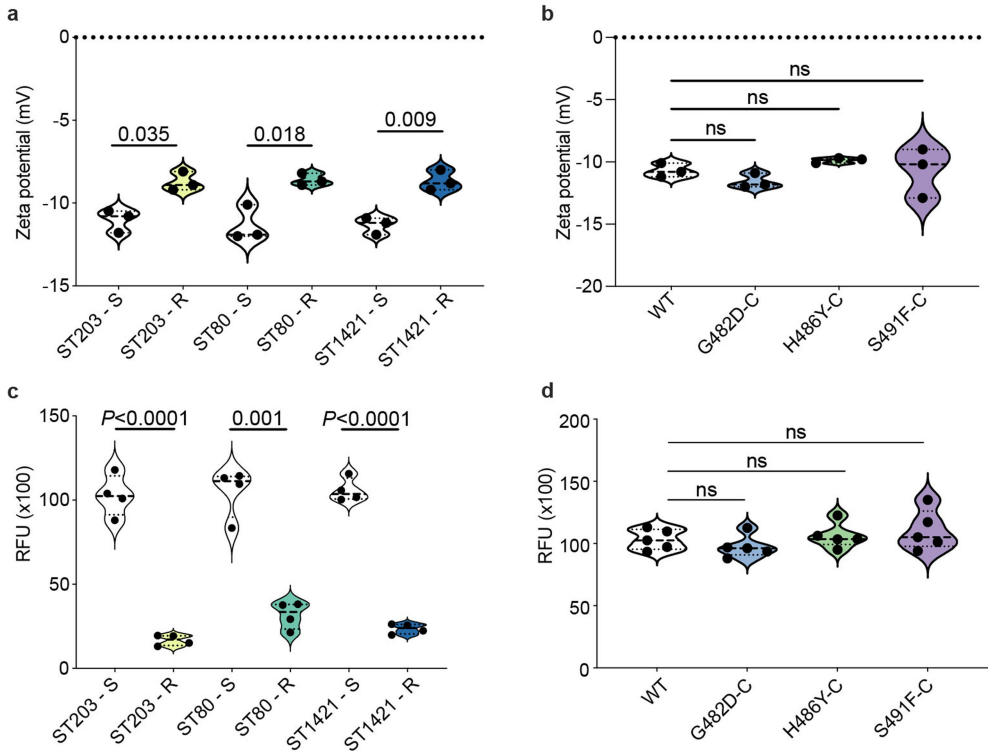

Extended Data Fig. 9 | Cell membrane charge and daptomycin binding. **a**-**b**. Zeta potential (measured in mV) is shown on the y-axis. Points represent each independent biological replicates (n = 3) and lines represent the median and interquartile range. Data was analysed with a one-way ANOVA [daptomycin-susceptible clinical strain versus daptomycin-resistant clinical strain (with a RpoB mutation) (ST203 [H486Y], ST80 [G482D], ST1421 [S491F]) or WT versus RpoB complement (-C)] and *P* values were corrected for multiple testing using the Dunnett method. **c**-**d**. Binding of BoDIPY-DAP, represented as relative fluorescence units (RFU) is shown on the y-axis. Points represent each independent biological replicates (n = 4 for the clinical strains and n = 5 for the RpoB complement strains) and lines represent the median and interquartile range. Data was analysed with a one-way ANOVA [daptomycin-susceptible clinical strain versus daptomycin-resistant clinical strain (with a RpoB mutation) (ST203 [H486Y], ST80 [G482D], ST1421 [S491F]) or WT versus RpoB complement (-C)] and *P* values were corrected for multiple testing using the Dunnett method. For **a**-**d** exact *P* values are provided when the *P* value is above $P < 0.0001$; ns=not significant.

nature portfolio

Corresponding author(s): Glen Carter

Last updated by author(s): Aug 14, 2024

Reporting Summary

Nature Portfolio wishes to improve the reproducibility of the work that we publish. This form provides structure for consistency and transparency in reporting. For further information on Nature Portfolio policies, see our Editorial Policies and the Editorial Policy Checklist.

Statistics

For all statistical analyses, confirm that the following items are present in the figure legend, table legend, main text, or Methods section.

n/a	Confirmed	
☐	☒	The exact sample size (*n*) for each experimental group/condition, given as a discrete number and unit of measurement
☐	☒	A statement on whether measurements were taken from distinct samples or whether the same sample was measured repeatedly
☐	☒	The statistical test(s) used AND whether they are one- or two-sided *Only common tests should be described solely by name; describe more complex techniques in the Methods section.*
☐	☒	A description of all covariates tested
☐	☒	A description of any assumptions or corrections, such as tests of normality and adjustment for multiple comparisons
☐	☒	A full description of the statistical parameters including central tendency (e.g. means) or other basic estimates (e.g. regression coefficient) AND variation (e.g. standard deviation) or associated estimates of uncertainty (e.g. confidence intervals)
☐	☒	For null hypothesis testing, the test statistic (e.g. *F*, *t*, *r*) with confidence intervals, effect sizes, degrees of freedom and *P* value noted *Give P values as exact values whenever suitable.*
☐	☒	For Bayesian analysis, information on the choice of priors and Markov chain Monte Carlo settings
☒	☐	For hierarchical and complex designs, identification of the appropriate level for tests and full reporting of outcomes
☐	☒	Estimates of effect sizes (e.g. Cohen's *d*, Pearson's *r*), indicating how they were calculated

Our web collection on statistics for biologists contains articles on many of the points above.

Software and code

Policy information about availability of computer code

Data collection	No software was used for data collection.
Data analysis	See Methods for settings used for all tools spades v.3.13 (https://github.com/ablab/spades) mlst v.2.19.0 (https://github.com/tseemann/mlst) snippy v.4.4.5 (https://github.com/tseemann/snippy) IQ-tree v.2.1.2 (https://github.com/Cibiv/IQ-TREE) R v.4.0.3 (https://www.r-project.org/) phangorn v.2.5.5 (https://github.com/KlausVigo/phangorn) ape v.5.4 (https://github.com/cran/ape) ggtree v.2.3.4 (https://github.com/YuLab-SMU/ggtree) ggplot2 v.3.3.2 (https://github.com/tidyverse/ggplot2) abriTAMR v.3.10.42 (https://github.com/MDU-PHL/abritamr) homoplasyFinder v.0.0.0.9 (https://github.com/JosephCrispell/homoplasyFinder) pyseer v.1.3.6 (https://github.com/mgalardini/pyseer) chewBBACA v.2.0.16 (https://github.com/B-UMMI/chewBBACA) COREugate v.2.0.4 (https://github.com/MDU-PHL/Coreugate) gubbins v.2.4.1 (https://github.com/nickjcroucher/gubbins) TempEst v.1.5 (https://beast.community/tempest) BEAST v.1.10.4 (https://beast.community/) SKA v.1.0 (https://github.com/simonrharris/SKA)

MS Dial v.4.90 (http://prime.psc.riken.jp/compms/msdial/main.html)
TrimGalore v.0.6.2 (https://github.com/FelixKrueger/TrimGalore)
BBDuk v.39.01 (https://github.com/BioInfoTools/BBMap)
Bowtie2 v.2.5.1 (https://github.com/BenLangmead/bowtie2)
htseq-count v.0.12.4 (https://github.com/simon-anders/htseq)
degust v.4.1.1 (https://github.com/drpowell/degust)
tidyverse v.1.3.1 (https://github.com/tidyverse)
patchwork v.1.1.1 (https://github.com/thomasp85/patchwork)
ggnewscale v.0.4.5 (https://github.com/eliocamp/ggnewscale)
GraphPad Prism v.9.3.1 (https://www.graphpad.com/)
BBDuk script in BBtools v.39.01 (https://sourceforge.net/projects/bbmap/)
Spectronaut v.16.0.220606.53000 (https://biognosys.com)
Perseus v.1.6.0.7 (https://maxquant.net)
Maestro Schrodinger suite release 2022-2 (https://www.schrodinger.com/release-download)
BLAST+ v2.15.0 (https://ftp.ncbi.nlm.nih.gov/blast/executables/blast+/2.15.0)
Dynamut2 v.1 (https://biosig.lab.uq.edu.au/dynamut2)
mmCSM-lig v.1(https://biosig.lab.uq.edu.au/mmcsm_lig/)
mmCSM-NA v.2 (https://biosig.lab.uq.au/mmcsm_na/)
mmCSM-PPI2 v.1(https://biosig.lab.uq.au/mcsm_ppi2/)

For manuscripts utilizing custom algorithms or software that are central to the research but not yet described in published literature, software must be made available to editors and reviewers. We strongly encourage code deposition in a community repository (e.g. GitHub). See the Nature Portfolio guidelines for submitting code & software for further information.

Data

Policy information about availability of data

All manuscripts must include a data availability statement. This statement should provide the following information, where applicable:

- Accession codes, unique identifiers, or web links for publicly available datasets
- A description of any restrictions on data availability
- For clinical datasets or third party data, please ensure that the statement adheres to our policy

Illumina sequencing reads for all samples and RNA sequencing data presented in the study are deposited under Bioprojects PRJNA565795, PRJNA433676, PRJNA856406. A full isolate list and associated metadata can be found in Supplementary Data 10. The mass spectrometry proteomics data has been deposited in the Proteome Xchange Consortium via the PRIDE partner repository with the data set identifier: PXD039832 and PXD039831.

Research involving human participants, their data, or biological material

Policy information about studies with human participants or human data. See also policy information about sex, gender (identity/presentation), and sexual orientation and race, ethnicity and racism.

Reporting on sex and gender	The sex of patients as determined from hospital medical records was included as a patient demographic in our retrospective cohort study to ensure the "control" and "test" groups were balanced. Sex based analyses were however not performed since patient sex was not relevant to our study design or outcomes.
Reporting on race, ethnicity, or other socially relevant groupings	Race, ethnicity and other socially relevant groupings were not included as patient demographics in our retrospective cohort study since these patient data were not relevant to our study design or outcomes.
Population characteristics	For the Melbourne cohort study, patients characteristics for the control group were as follows: female 45%, male 55%; median age: 66 yo; median Charleston Comorbidity Index: 3; Reported comorbidities: Ischemic heart disease, cardiac failure, peripheral vascular disease, cerebrovascular disease, cognitive impairment, hemiplegia, chronic obstructive pulmonary disease, autoimmune/ connective tissue disease, diabetes, peptic ulcer disease, chronic liver disease, chronic kidney disease, solid organ cancer, leukaemia/ lymphoma and immunocompromised; Rifaximin exposure in the last 90 days: No; Other antimicrobial exposure in the last 90 days: Yes. For the rifaximin group, patient characteristics were as follows: Female 44%, make 56%; median age: 57 yo; median Charleston Index: 4; Reported comorbidities: Ischaemic heart disease, cardiac failure, peripheral vascular disease, cerebrovascular disease, cognitive impairment, chronic obstructive pulmonary disease, autoimmune/connective tissue disease, diabetes, peptic ulcer disease, chronic liver disease, chronic kidney disease, solid organ cancer, leukaemia/ lymphoma, immunocompromised; Rifaximin exposure in the last 90 days: Yes; Other antimicrobial exposure in the last 90 days: Yes. Detailed descriptions of patient demographics associated with this cohort are available in Supplementary Table 2 and 4A. For the Regensburg cohort, patient characteristics for the control group were: HSCT recipient: Yes; sex: female 32%, male 68%; median age: 54 yo; underlying haematological diagnoses: Acute leukaemia, myelodysplastic syndrome, myeloproliferative syndrome, non-Hodgkin's lymphoma/ myeloma; Rifaximin prophylaxis: No; Other antimicrobial exposure: Yes. For the Rifaximin group, patient characteristics were: HSCT recipient: Yes; sex: female 37%, male 63%; median age: 55 yo; underlying haematological diagnoses: Acute leukaemia, myelodysplastic syndrome, non-Hodgkin's lymphoma/ myeloma; Rifaximin prophylaxis: Yes; Other antimicrobial exposure: Yes. Detailed descriptions of patient demographics associated with this cohort are available in Supplementary Table 6A and 6B.
Recruitment	Patients were not recruited for this work. Both independent studies were retrospective cohort studies. Medical records of patients from whom VREfm isolates were collected were accessed by clinical investigators associated with the study. There was no patient selection bias.

Ethics oversight	For the Melbourne cohort study, data were obtained from medical records with approval from the Austin Health Human Research Ethics Committee (HREC/92971/Austin-2023), which included a waiver of consent in accordance with the National Statement on Ethical Conduct in Human Research 2023 (Australia). For the Regensburg cohort study, data were obtained from medical records with approval from the local ethics committee (ethical committee of the University of Regensburg - 21-2521-101). Stool samples were collected from patients after obtaining written informed consent and the study was performed in accordance with the Declaration of Helsinki

Note that full information on the approval of the study protocol must also be provided in the manuscript.

Field-specific reporting

Please select the one below that is the best fit for your research. If you are not sure, read the appropriate sections before making your selection.

☒ Life sciences ☐ Behavioural & social sciences ☐ Ecological, evolutionary & environmental sciences

For a reference copy of the document with all sections, see nature.com/documents/nr-reporting-summary-flat.pdf

Life sciences study design

All studies must disclose on these points even when the disclosure is negative.

Sample size	Group sizes for animal experiments were calculated using a power of 80%, an attrition rate of 15% and a type I error of 5%. these parameters were based extensive previous experience of using each animal model. For the human cohort studies no sample size calculations were performed due to the retrospective nature of the studies. It is well reported in the literature that post hoc sample size calculations for retrospective studies are not robust. Instead, retrospective studies like ours rely on effect size and confidence intervals to assess whether the cohort is large enough. Our large effect size and narrow confidence intervals demonstrate the cohort sizes used in our analyses are large enough to provide robust and accurate data.
Data exclusions	No data was excluded from the study
Replication	All experimentation was performed with at least 3 independent biological replicates. The number of replicates for each experiment is stated in the associated methods/figure legend. In all cases biological repeats were successful. No discrepancies between repeats were encountered.
Randomization	When multiple bacterial isolates were collected from a single patient, the isolate included in our cohort studies was randomised. To do this one investigator gave isolates an untraceable, non-sequential identifier and a second investigator then chose the identifier to be included in the cohort study. For all animal experiments, mice were randomly assigned to cages upon arrival from the breeding facility by animal facility technicians that were not involved in the study. After acclimatisation, cages were randomly assigned to treatment (or control) groups by the researchers performing the experiments using numerical cage identifiers assigned by the animal facility technicians on arrival. The selection of VREfm isolates collected from mouse stool samples for WGS was randomised within each group. To do this the researcher performing the experiment streaked isolates collected from each mouse onto agar grids, with each streak within the grid being numbered (1-50). Isolates were then selected for WGS based on their number within the grid, which were picked according to numbers generated using a free online random number generator available at calculatorsoup.com.
Blinding	The investigator perfoming all analyses associated with the retrospective cohort studies was blinded to the cohort groups. To achieve this one investigator allocated isolates to the appropriate cohort groups, and then de-identified the groups. A second investigator then performed all analyses on the de-identified groups. When analysing VREfm in stool samples collected from mice receiving either rifamycins, daptomycin or vehicles, the researcher was blinded to the experimental group that the stool samples were collected from. This was achieved by one researcher collecting stool samples into de-identified tubes and a second resercher then isolating and characterising VREfm from the stool in each de-identified tube. However, subsequent selection of isolates for WGS was not blinded since we had to ensure that an equal number of isolates from each group and at the desired time points were sequenced. Blinding would have made this impossible.

Reporting for specific materials, systems and methods

We require information from authors about some types of materials, experimental systems and methods used in many studies. Here, indicate whether each material, system or method listed is relevant to your study. If you are not sure if a list item applies to your research, read the appropriate section before selecting a response.

Materials & experimental systems

n/a	Involved in the study
☒	☐ Antibodies
☒	☐ Eukaryotic cell lines
☒	☐ Palaeontology and archaeology
☐	☒ Animals and other organisms
☒	☐ Clinical data
☐	☒ Dual use research of concern
☒	☐ Plants

Methods

n/a	Involved in the study
☒	☐ ChIP-seq
☒	☐ Flow cytometry
☒	☐ MRI-based neuroimaging

Animals and other research organisms

Policy information about studies involving animals; ARRIVE guidelines recommended for reporting animal research, and Sex and Gender in Research

Laboratory animals	Female C57BL/6 mice at age 6-8 weeks were purchased from WEHI and used in the study. Mice were maintained in an SPF-facility at the Peter Doherty Institute. The facility operates a 12h light/ 12h dark cycle and maintains ambient tempertaure (18 - 23C) and humidity (40 - 60%). Animals were fed a standard mouse chow diet and provided with water ad libitum.
Wild animals	The study did not involve wild animals
Reporting on sex	The findings are applicable to both male and female animals. There is no sex bias in the outcomes of our animal experiments, with past experience showing that the both male and female animals give identical outcomes in the animal models used. All experiments were performed with female mice. The sex of animals was not a consideration in the design of the experiments used in this study as it does not influence experimental outcomes in the model.
Field-collected samples	The study did not include samples collected from the field
Ethics oversight	All animal experimentation was approved by the University of Melbourne Animal Ethics Committee (application IDs: 20094 and 28528).

Note that full information on the approval of the study protocol must also be provided in the manuscript.

Dual use research of concern

Policy information about dual use research of concern

Hazards

Could the accidental, deliberate or reckless misuse of agents or technologies generated in the work, or the application of information presented in the manuscript, pose a threat to:

No	Yes	
☒	☐	Public health
☒	☐	National security
☒	☐	Crops and/or livestock
☒	☐	Ecosystems
☒	☐	Any other significant area

Experiments of concern

Does the work involve any of these experiments of concern:

No	Yes	
☐	☐	Demonstrate how to render a vaccine ineffective
☐	☒	Confer resistance to therapeutically useful antibiotics or antiviral agents
☐	☐	Enhance the virulence of a pathogen or render a nonpathogen virulent
☐	☐	Increase transmissibility of a pathogen
☐	☐	Alter the host range of a pathogen
☐	☐	Enable evasion of diagnostic/detection modalities
☐	☐	Enable the weaponization of a biological agent or toxin
☐	☐	Any other potentially harmful combination of experiments and agents